

## Southern Argentina Agile Meteor Radar: Initial assessment of gravity wave momentum fluxes

D. C. Fritts,<sup>1</sup> D. Janches,<sup>1</sup> and W. K. Hocking<sup>2</sup>

Received 20 January 2010; revised 18 May 2010; accepted 20 May 2010; published 13 October 2010.

[1] The Southern Argentina Agile Meteor Radar (SAAMER) was installed on Tierra del Fuego (53.8°S) in May 2008 and has been operational since that time. This paper describes tests of the SAAMER ability to measure gravity wave momentum fluxes and applications of this capability during different seasons. Test results for specified mean, tidal, and gravity wavefields, including tidal amplitudes and gravity wave momentum fluxes varying strongly with altitude and/or time, suggest that the distribution of meteors throughout the diurnal cycle and averaged over a month allows characterization of both monthly mean profiles and diurnal variations of the gravity wave momentum fluxes. Applications of the same methods for real data suggest confidence in the monthly mean profiles and the composite day diurnal variations of gravity wave momentum fluxes at altitudes where meteor counts are sufficient to yield good statistical fits to the data. Monthly mean zonal winds and gravity wave momentum fluxes exhibit anticorrelations consistent with those seen at other midlatitude and high-latitude radars during austral spring and summer, when no strong local gravity wave sources are apparent. When stratospheric variances are significantly enhanced over the Drake Passage “hot spot” during austral winter, however, MLT winds and momentum fluxes over SAAMER exhibit very different correlations that suggest that MLT dynamics are strongly influenced by strong local gravity wave sources within this “hot spot.” SAAMER measurements of mean zonal and meridional winds at these times and their differences from measurements at a conjugate site provide further support for the unusual momentum flux measurements.

**Citation:** Fritts, D. C., D. Janches, and W. K. Hocking (2010), Southern Argentina Agile Meteor Radar: Initial assessment of gravity wave momentum fluxes, *J. Geophys. Res.*, 115, D19123, doi:10.1029/2010JD013891.

### 1. Introduction

[2] *Fritts et al.* [2010, hereafter F10] describe the motivation for the design and placement of the Southern Argentina Agile Meteor Radar (SAAMER) at Rio Grande on Tierra del Fuego (53.8°S, 67.8°W), which became operational in May 2008, as well as its characterization of the mean and tidal motions and planetary wave (PW) influences throughout its first year of operation. An important motivation for the design of SAAMER, in particular the high power (60 kW) and the transmitting antenna creating eight beams with peak power at ~35° off zenith and most meteor counts between 15° and 50° off zenith, was the hope that this design would enable SAAMER to measure mesosphere and lower thermosphere (MLT) gravity wave (GW) momentum fluxes and their modulation by variable mean, tidal, and PW motions. Such direct measurements have only been possible previously with radars or lidars having symmetric, relatively

narrow, off-zenith coplanar beam pairs [*Vincent and Reid*, 1983; *Reid and Vincent*, 1987; *Fritts and Vincent*, 1987; *Fukao et al.*, 1988; *Reid et al.*, 1988; *Fritts and Yuan*, 1989; *Fritts et al.*, 1990, 1992; *Sato*, 1990, 1993, 1994; *Tsuda et al.*, 1990; *Wang and Fritts*, 1990, 1991; *Hitchman et al.*, 1992; *Nakamura et al.*, 1993; *Murayama et al.*, 1994; *Murphy and Vincent*, 1998; *Acott*, 2009]. Our purposes in this paper are (1) to evaluate the ability of SAAMER to measure GW momentum fluxes, given the annual, diurnal, and spatial variability in the meteor detections shown by F10, and (2) to apply this capability in monthly assessments of mean momentum flux profiles and their diurnal modulation by monthly mean tidal structures. Indeed, the method appears to work for altitudes and intervals for which there are sufficient meteor counts in opposing coplanar directions for each hour of the composite days.

[3] Our evaluation of SAAMER measurement accuracy for constant and spatially and temporally variable mean, tidal, and GW fields is described in section 2. Section 3 describes monthly mean winds, diurnal and semidiurnal tides, and GW momentum fluxes, the daily variations of winds, and the diurnal variations of winds and momentum fluxes throughout a composite day for each month analyzed. Section 4 discusses similarities of SAAMER results to and differences from those

<sup>1</sup>NorthWest Research Associates, Colorado Research Associates Division, Boulder, Colorado, USA.

<sup>2</sup>Department of Physics, University of Western Ontario, London, Ontario, Canada.

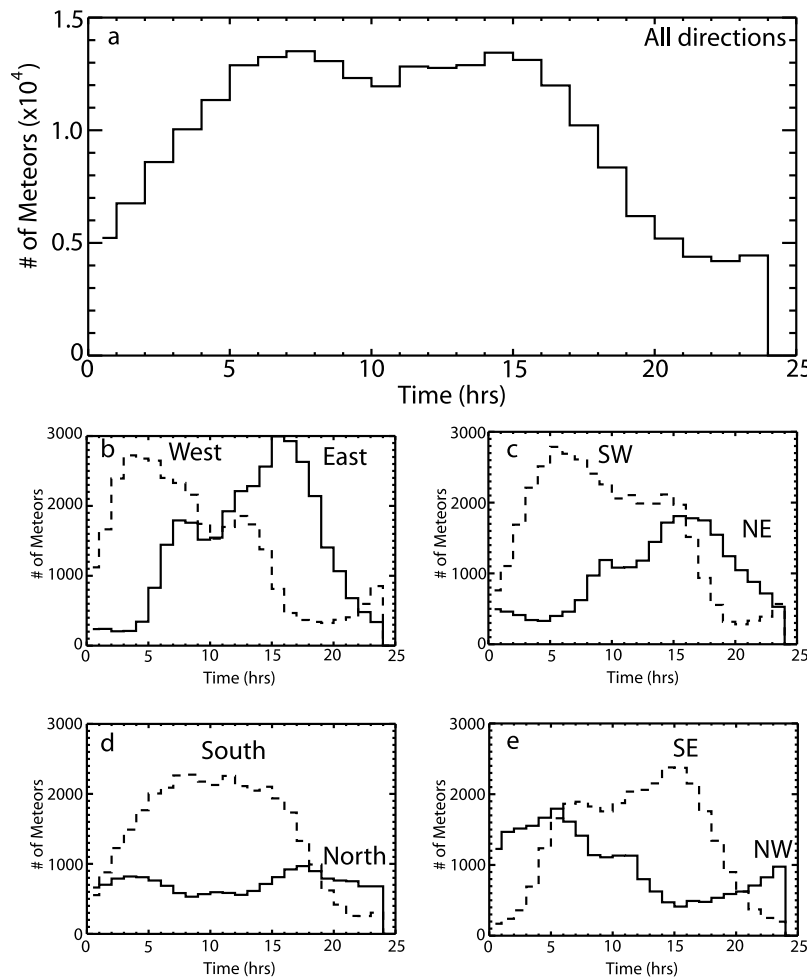


**Figure 1.** (a) Mean diurnal meteor occurrence with local time (LT) and (b–e) valid meteor detections binned by hour for September 2008 for each of the primary SAAMER beams (in opposing beam pairs). A pronounced minimum in detections rotates counterclockwise (viewing downward) throughout the diurnal cycle.

at other sites and other SAAMER measurements that provide additional verification of these results. Our summary and conclusions are provided in section 5.

## 2. Evaluation of SAAMER GW Momentum Flux Measurement Capabilities

[4] Our SAAMER system description and initial study of seasonal variations of mean winds and tides by F10 revealed ~40% variations in meteor fluxes throughout the year. It also revealed a peak meteor flux at ~90 km, decreasing to ~50% of maximum at ~84 and 96 km and ~20% of maximum at ~79 and 99 km. On the basis of previous observations and meteor radiant modeling [Janches *et al.*, 2004, 2006], we anticipated significant diurnal variations of meteor detections at different azimuths. This was observed at SAAMER and posed the greatest challenge to our hope that SAAMER would yield sufficient simultaneous meteor counts in opposite beam directions to enable valid momentum flux estimates. Diurnal variability of total meteor detections and separately in the eight primary radar beams (between 15° and 50° off zenith) for a composite day (i.e., averaged over 30 days for each hour of local time, or LT) during

September 2008 is shown in Figure 1. As expected, there are significant diurnal variations (with similar variations in other months), with binned hourly totals of unambiguous meteor detections ranging from near ~400 to 1400/h during each month during these initial observations. The minimum count rate equates to ~10 meteors/3 km altitude bin/beam/h and is likely much too small to allow GW momentum flux estimates for intervals less than a day or so. While daily or several day estimates may prove possible with further analysis, we choose to be conservative initially and consider only monthly averages here for which there are large numbers of meteor detections at all azimuths and zenith angles at the altitudes having the higher count rates. Thus, we demonstrate below that SAAMER achieves sufficient meteor counts to yield valid GW momentum flux estimates for various test mean, tidal, and GW fields, and apparently significant, but credible, monthly estimates for real data during different seasons. Our analysis here employs the S transform [Stockwell *et al.*, 1996] used by F10 to determine mean and tidal structures and the “full-field” statistical meteor analysis of Hocking [2005] for GW momentum flux estimates for the residual fields (after mean and tidal removal) employing monthly composites to increase meteor statistics.

The procedure described by *Hocking* [2005] can be viewed as a generalization of the dual-beam method devised by *Vincent and Reid* [1983] and its extension to multiple beams by *VanZandt et al.* [1990] and *Fritts et al.* [1990].

### 2.1. Specification of Test Mean, Tidal, and GW Fields

[5] To evaluate the potential for SAAMER meteor counts and distributions to allow assessments of GW momentum fluxes, we employ real meteor spatial and temporal distributions observed by SAAMER during September 2008 with various specified (and superposed) mean, tidal, and GW velocity fields for both constant and spatially and temporally variable tidal and GW amplitudes that are intended to be representative of the scales, amplitudes, and momentum fluxes of such motions at this location. We then compare the monthly mean fields, the daily mean winds, and composite day hourly variability, where appropriate, to assess where SAAMER can be expected to provide sufficiently accurate estimates in real observations. These test fields are intended to include increasing degrees of realism and complexity and are assumed to have the following structures,

$$\begin{aligned}
 U(x,y,z,t) = & U_M + U_D(z,t) \sin(2\pi t/T_D) + U_{SD}(z,t) \sin(2\pi t/T_{SD}) \\
 & + U_{GW1}(x,y,z,t) \sin(k_1x + l_1y + m_1z - 2\pi t/T_{GW1}) \\
 & + U_{GW2}(x,y,z,t) \sin(k_2x + l_2y + m_2z - 2\pi t/T_{GW2}) \\
 & + U_{GW3}(x,y,z,t) \sin(k_3x + l_3y + m_3z - 2\pi t/T_{GW3}),
 \end{aligned} \tag{1}$$

$$\begin{aligned}
 V(x,y,z,t) = & V_M - V_D(z,t) \cos(2\pi t/T_D) - V_{SD}(z,t) \cos(2\pi t/T_{SD}) \\
 & + V_{GW1}(x,y,z,t) \sin(k_1x + l_1y + m_1z - 2\pi t/T_{GW1}) \\
 & + V_{GW2}(x,y,z,t) \sin(k_2x + l_2y + m_2z - 2\pi t/T_{GW2}) \\
 & + V_{GW3}(x,y,z,t) \sin(k_3x + l_3y + m_3z - 2\pi t/T_{GW3}),
 \end{aligned} \tag{2}$$

$$\begin{aligned}
 W(x,y,z,t) = & W_{GW1}(x,y,z,t) \sin(k_1x + m_1z - 2\pi t/T_{GW1}) \\
 & + W_{GW2}(x,y,z,t) \sin(k_2x + l_2y + m_2z - 2\pi t/T_{GW2}) \\
 & + W_{GW3}(x,y,z,t) \sin(k_3x + l_3y + m_3z - 2\pi t/T_{GW3}).
 \end{aligned} \tag{3}$$

[6] These include the following:

[7] 1. zonal and meridional mean winds,  $U_M$  and  $V_M$ ;

[8] 2. diurnal and semidiurnal tides having zonal and meridional amplitudes of  $(U_D, V_D)$  and  $(U_{SD}, V_{SD})$  assumed to rotate counterclockwise with time and which may have either constant or varying amplitudes with increasing altitude;

[9] 3. traveling GWs having amplitudes  $(U_{GW}, V_{GW}, W_{GW})$ , zonal, meridional, or oblique propagation, spatial and temporal variability, correlated horizontal and vertical motions, and constant or variable momentum fluxes; and

[10] 4. stationary mountain waves (MWs) having zonal and meridional propagation, only spatial variability, correlated horizontal and vertical motions, and constant momentum fluxes.

[11] The mean, tidal, and GW amplitudes and spatial and temporal parameters are listed in Table 1 for each of the test cases considered. Results for each case are discussed further below.

### 2.2. Evaluation of SAAMER Measurement Capabilities

[12] Our purpose in this section is to assess how well SAAMER performs in describing specified large-scale motions and GW momentum fluxes of increasing realism and complexity when sampled with the spatial and temporal distribution of meteors observed during September 2008 shown in Figure 1. Mean winds, diurnal and semidiurnal tidal amplitudes, and GWs having prescribed spatial and/or temporal variability and momentum fluxes propagating zonally, meridionally, or at other azimuths are defined by equations (1)–(3) and the seven cases listed in Table 1. Specified (i.e., defined by equations (1)–(3) and Table 1) and recovered (i.e., the velocity fields inferred from our S transform and Hocking statistical analysis) profiles of the mean winds, diurnal and semidiurnal tides, and GWs momentum fluxes, and their daily and composite day hourly variability, where appropriate, are discussed separately for each case below.

#### 2.2.1. Case 1

[13] Specified and recovered fields for Case 1, using actual meteor distributions in space and time for September 2008 to estimate these fields, are shown as monthly means in Figure 2. In this case, the tides were assumed to have only temporal variations and the GWs only horizontal variations, with 50 and 100 km wavelengths in the zonal and meridional motions, respectively (see Table 1). These reveal excellent agreement, with mean winds and tidal amplitudes accurate to  $\sim 2\%$  or better except at the lowest altitude (and at 97.5 km, not shown), and GW momentum flux estimates that are likewise accurate to  $\sim 5\%$  or better, except for an  $\sim 8\%$  departure of the zonal momentum flux estimate at 94.5 km, where meteor counts are decreasing and tidal modulation is large. These results suggest an impressive ability of SAAMER to describe both the large-scale wind fields (including tides) and GW momentum fluxes for conditions in which these fields are uniform throughout the month and meteor detection rates are sufficiently large.

#### 2.2.2. Case 2

[14] Case 2 includes no mean winds or tides and only a zonal stationary GW with prescribed horizontal and vertical phase variations (with wavelengths of 50 and 15 km, see Table 1). The specified and recovered motions reveal very small mean and tidal amplitudes (not shown) and GW momentum fluxes (Figure 3, top) again within  $\sim 2\%$  of the specified nonzero zonal value ( $50 \text{ m}^2 \text{ s}^{-2}$ ) and at most  $\sim 0.5 \text{ m}^2 \text{ s}^{-2}$  different from the specified zero meridional value. Thus, SAAMER also apparently has the ability to isolate momentum fluxes when these occur for only one direction of GW propagation, when the motion is steady, and has vertical phase variation.

#### 2.2.3. Case 3

[15] Case 3 considers a motion field with no mean winds or tides, but with both zonal and meridional stationary GWs, having horizontal wavelengths of 30 and 40 km, respectively, but no vertical phase variations (see Table 1). Mean momentum fluxes (Figure 3, bottom) are again in close agreement with specified values. As seen above, SAAMER appears to have an ability to define orthogonal motions and momentum fluxes arising from GWs having different spatial scales and orientations, whether they are propagating or stationary.

**Table 1.** Mean, Tidal, and GW Parameters Used for Test Cases Evaluating SAAMER Measurement Capabilities Employing Real Meteor Distributions and Test Motion Fields<sup>a</sup>

| Parameter                            | Case 1     | Case 2    | Case 3    | Case 4     | Case 5  | Case 6     | Case 7      |
|--------------------------------------|------------|-----------|-----------|------------|---|------------|-------------|
| $U_M, V_M$                           | 20, 10     | 0, 0      | 0, 0      | 20, 10     | 40, -20   | -20, -10   | -20, -10    |
| $U_D, V_D$                           | 10, 10     | 0, 0      | 0, 0      | 10, 10     | 20, 20  | 10, 10     | 10, 10      |
| $U_{SD}, V_{SD}$                     | 50, 50     | 0, 0      | 0, 0      | 50, 50     | $20 + 2(z - 80)\sin^2(\pi t/T_M)$                                     | 50, 50     | 50, 50      |
| $U_{GW1}$                            | 10         | 20        | 20        | 10         | $20 \text{ abs}[\sin(2\pi t/T_M)] * \sin(2\pi t/T_{SD})$              | $40F_6(t)$ | $30F_7(t)$  |
| $V_{GW1}$                            | 0          | 0         | 0         | 0          | 0   | 0          | $30F_7(t)$  |
| $W_{GW1}$                            | 5          | 5         | -10       | 5          | 0   | $20F_6(t)$ | $10F_7(t)$  |
| $k_1$                                | $2\pi/50$  | $2\pi/50$ | $2\pi/30$ | $2\pi/50$  | $-10 \text{ abs}[\sin(2\pi t/T_M)] * \text{abs}[\sin(2\pi t/T_{SD})]$ | $2\pi/50$  | $2\pi/40$   |
| $l_1$                                | 0          | 0         | 0         | 0          | 0   | 0          | $2\pi/40$   |
| $m_1$                                | 0          | $2\pi/15$ | 0         | 0          | $2\pi/50$   | $2\pi/15$  | $2\pi/15$   |
| $T_{GW1}$                            | 20         | $\infty$  | $\infty$  | 20         | 0   | 20         | 20          |
|                                      |            |           |           |            | 0   |            |             |
|                                      |            |           |           |            | 20  |            |             |
| $U_{GW2}$                            | 0          | -         | 0         | 0          | 0   | 0          | $30G_7(t)$  |
| $V_{GW2}$                            | 20         |           | 10        | 20         | $20 \text{ abs}[\sin(2\pi t/T_M)] * \cos(2\pi t/T_{SD})$              | $30G_6(t)$ | $-30G_7(t)$ |
| $W_{GW2}$                            | 2          |           | 2         | 2          |   | $10G_6(t)$ | $20G_7(t)$  |
| $k_2$                                | 0          |           | 0         | 0          | $5 \text{ abs}[\sin(2\pi t/T_M)] * \text{abs}[\cos(2\pi t/T_{SD})]$   | 0          | $2\pi/50$   |
| $l_2$                                | $2\pi/100$ |           | $2\pi/40$ | $2\pi/100$ |   | $2\pi/100$ | $2\pi/50$   |
| $m_2$                                | 0          |           | 0         | 0          | 0   | $2\pi/20$  | $2\pi/20$   |
| $T_{GW2}$                            | 30         |           | $\infty$  | 30         | $2\pi/100$  | 30         | 15          |
|                                      |            |           |           |            | 0   |            |             |
|                                      |            |           |           |            | 30  |            |             |
| $U_{GW3}$                            | -          | -         | -         | 20         | 20  | -          | -           |
| $W_{GW3}$                            |            |           |           | -10        | -10   |            |             |
| $k_3$                                |            |           |           | $2\pi/30$  | $2\pi/30$   |            |             |
| $m_3$                                |            |           |           | 0          | 0   |            |             |
| $T_{GW3}$                            |            |           |           | $\infty$   | $\infty$  |            |             |
| $V_{GW4}$                            | -          | -         | -         | 10         | 10  | -          | -           |
| $W_{GW4}$                            |            |           |           | 2          | 2   |            |             |
| $l_4$                                |            |           |           | $2\pi/40$  | $2\pi/40$   |            |             |
| $m_4$                                |            |           |           | 0          | 0   |            |             |
| $T_{GW4}$                            |            |           |           | $\infty$   | $\infty$  |            |             |
| $\langle u'w' \rangle_{\text{mean}}$ | 25         | 50        | -100      | -75        | -100  | 50         | 75          |
| $\langle v'w' \rangle_{\text{mean}}$ | 20         | 0         | 10        | 30         | 10  | 25         | -25         |

<sup>a</sup>Daily-mean GW momentum fluxes for each case are shown at the bottom. Units for velocities, wave numbers, and periods are  $\text{m s}^{-1}$ ,  $\text{km}^{-1}$ , and min, and  $T_M = 10$  days and  $T_{SD} = 12$  h. GWs in Case 6 are modulated by amplitude functions  $F_6(t) = 1$  ( $t = 0-3$  h +  $21R_1$  h) and  $F_6(t) = 0$  otherwise, and  $G_6(t) = 1$  ( $t = 0-4$  h +  $20R_2$  h) and  $G_6(t) = 0$  otherwise, with  $R_1$  and  $R_2$  random variables between 0 and 1 chosen separately for each of the 30 days of the test month. GWs in Case 7 are modulated by amplitude functions  $F_7(t) = 1$  ( $t = 0-2$  and  $8-10$  h +  $14R_3$  h) and  $F_7(t) = 0$  otherwise, and  $G_7(t) = 1$  ( $t = 0-1$  h and  $6-7$  h and  $10-11$  h and  $19-20$  h +  $4R_4$  hr) and  $G_7(t) = 0$  otherwise, with  $R_3$  and  $R_4$  random variables between 0 and 1 as above.

#### 2.2.4. Case 4

[16] We now consider a more complex superposition of mean, tidal, and GW fields given by the sum of the various motions defined in Cases 1 and 3 (see Table 1). This includes zonal and meridional mean, tidal, and both stationary and propagating GW motions, with all amplitudes and GW momentum fluxes that are nevertheless constant in time. This case differs from the previous cases in that both zonal and meridional momentum fluxes now have contributions from stationary and propagating GWs having different spatial structures. As in Cases 1 and 3 individually, SAAMER recovers the mean winds, tidal amplitudes, and total GW momentum fluxes very well (see Figure 4), considering the now much more complex superposition of motions. Differences between the specified and recovered values are nevertheless somewhat larger for the larger superposition in Case 4, but with mean wind and tidal amplitude estimates still accurate to within  $\sim 1 \text{ m s}^{-1}$  or less except at the lowest (76.5 km) and highest altitudes (97.5 km, not shown). GW momentum flux differences are likewise slightly larger for Case 4, but still  $\sim 2 \text{ m}^2 \text{ s}^{-2}$  or less from 76.5 to 91.5 km, with errors increasing to  $\sim 5$  to  $7 \text{ m}^2 \text{ s}^{-2}$  at 94.5 km. These remain very encouraging comparisons to us, suggesting that SAAMER may have significant value in diagnosing large-scale motions and GW momentum fluxes for monthly mean

conditions at the least. Case 5 below explores SAAMER measurement capabilities when both tidal and GW motions exhibit significant spatial and temporal variability, as is often seen in our various MLT measurements.

#### 2.2.5. Case 5

[17] Case 5 explores a superposition of larger mean winds, a larger but constant diurnal tide, a semidiurnal tide that exhibits both a 10 day amplitude modulation and amplitude growth with altitude, and superposed GWs having zonal and meridional propagation. Both zonal and meridional GWs include (1) a propagating GW modulated in amplitude and its direction of propagation (and momentum flux magnitude and sign) by the semidiurnal tide and (2) a stationary GW with constant amplitude and momentum flux. Tidal components and GWs have no specified vertical phase variations, as we expect the SAAMER recovered motions to be independent at each altitude. All four GWs have different horizontal wavelengths (i.e., 30, 40, 50, and 100 km), however, to allow evaluation of the SAAMER ability to describe the resulting momentum flux for multiple GWs having different spatial and temporal structures and orientations.

[18] Mean and composite day results for Case 5 are shown in Figure 5 and reveal monthly mean winds and diurnal tide amplitudes that are again accurate to within  $\sim 1 \text{ m s}^{-1}$  or less, except where meteor detection rates are small (76.5 and

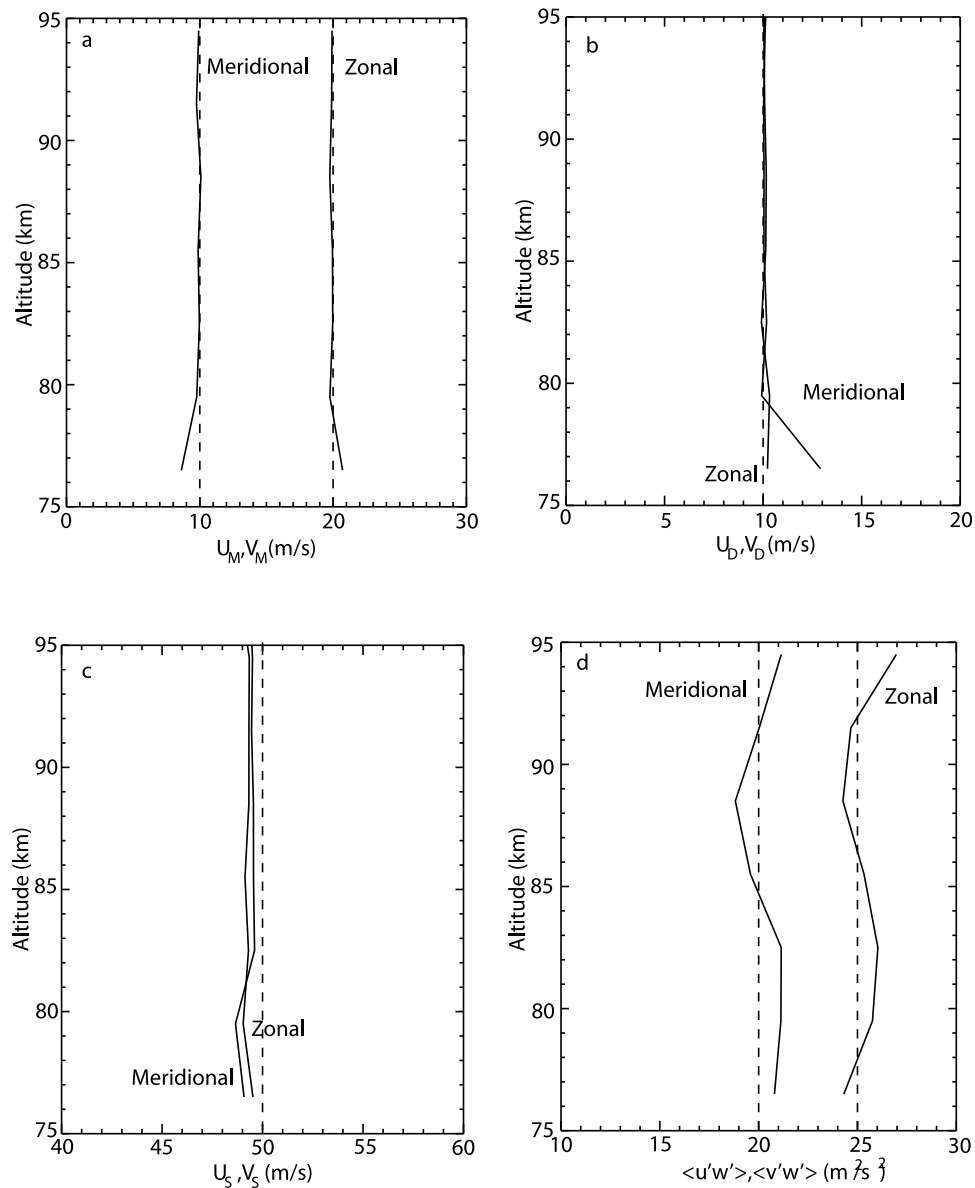


**Figure 2.** Monthly specified (dashed) and recovered (solid) distributions of (a) zonal and meridional mean winds, (b) diurnal tide amplitudes, (c) semidiurnal tide amplitudes, and (d) GW momentum fluxes for mean, tidal, and GW fields specified in Case 1. Note that the recovered amplitudes are within  $\sim 2\%$  for mean winds and tidal amplitudes and  $\sim 5\%$  for GW momentum fluxes except where meteor detection rates were very small. Recovered amplitudes and momentum fluxes were obtained with actual September 2008 meteor distributions.

97.5 km, the latter not shown). The second frames in each column show the zonal and meridional semidiurnal tide as a function of time at each altitude from 76.5 to 97.5 km for a composite day (results are averaged by hour for the meteor distribution observed during September 2008). The recovered amplitudes (solid lines) agree extremely well with the specified amplitudes (dashed lines) for all altitudes except 76.5 km in the meridional component, where the meteor detection rate is quite small. Even at 97.5 km, where meteor detection rates are also much smaller than at intermediate altitudes, SAAMER appears to capture the semidiurnal tide amplitude and phase very well.

[19] GW momentum fluxes for the modulated (and propagating) GWs in the zonal and meridional directions (GW1 and GW2 in Table 1 and excluding the stationary GW3 and GW4) are shown at left and right in the third frames of each column in Figure 5, with solid and dashed lines for the recovered and specified fields, respectively. The specified variations are not simply sinusoids, as individual modulated GW amplitudes are sinusoids having a semidiurnal periodicity. The corresponding momentum fluxes,  $\langle u'w' \rangle$  and  $\langle v'w' \rangle$  (with angle brackets denoting averaging), vary as  $\sin^2(2\pi/T_{SD} + \phi)$ , where  $T_{SD} = 12$  h,  $\phi$  accounts for the appropriate zonal or meridional phase, and the momentum flux sign changes oppositely to the corresponding tidal wind

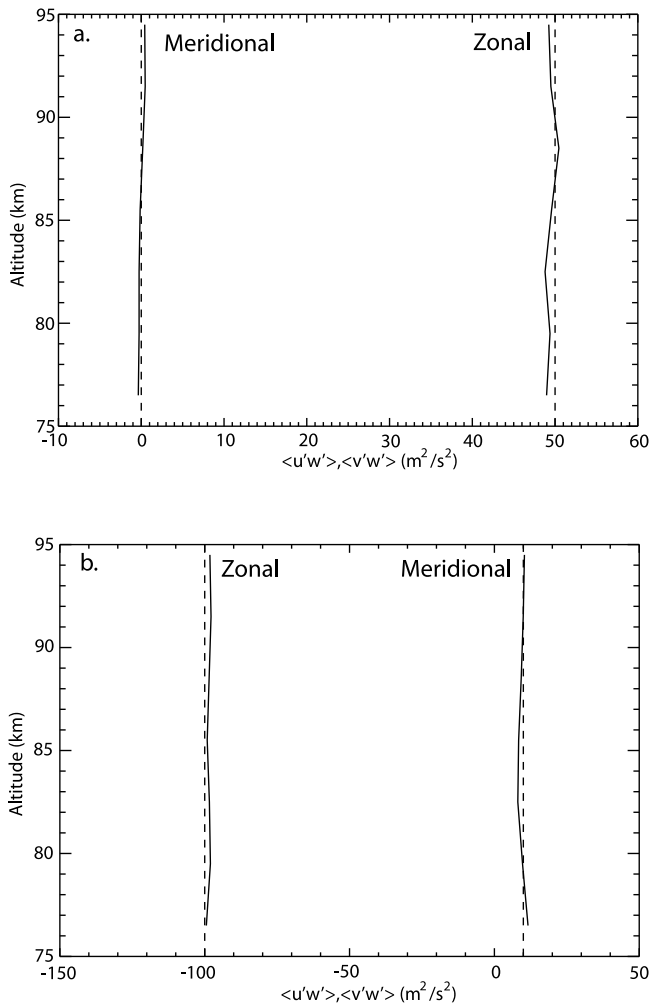


**Figure 3.** As in Figure 2, but for the GW momentum fluxes specified in Cases 2 and 3 (a and b), with a stationary zonal GW with altitude variations in Case 2 and stationary zonal and meridional GWs without altitude variations in Case 3. In this case, recovered large zonal momentum fluxes are within  $\sim 2\%$  of specified values, while small meridional momentum fluxes exhibit comparable errors, typically  $\sim 1\text{--}2\text{ m}^2\text{ s}^{-2}$ , but these are larger fractions of the much smaller mean meridional fluxes.

field. The recovered momentum fluxes are much coarser fits to the specified fields than for the semidiurnal tide components, especially at 76.5 km, for reasons discussed above. They nevertheless are quite accurate at altitudes where meteor detection rates are high, i.e., from 79.5 to 94.5 km.

[20] Consider now the momentum fluxes for the composite day including all four GWs specified for Case 5 in Table 1 (Figure 5, bottom). These composite momentum flux estimates are distinctly less accurate than without the superposed stationary GWs having zonal and meridional propagation, especially at the lowest and highest altitudes displayed. Estimates at the four intermediate altitudes (82.5–91.5 km) still track the specified values very well, but also exhibit significantly larger uncertainties than seen above,  $\sim 10\%\text{--}20\%$  at the extremes of the tidal modulations. Results at lower and higher altitudes exhibit further degraded quantitative agreement but

still display clear anticorrelations with the semidiurnal tide structures.

[21] The ability of SAAMER to determine daily mean winds and tidal amplitudes is displayed in Figure 6, in which the top frames show superposed daily zonal and meridional mean winds and diurnal tide amplitudes and the bottom frames show the temporal evolution of the semidiurnal tide amplitudes, with the specified amplitudes as dashed lines and the recovered amplitudes as solid lines in each case. RMS errors are a few  $\text{m s}^{-1}$  or less for all estimates, except at the lowest and highest altitudes (76.5 and 97.5 km), where meteor detection rates are very small.

[22] To further quantify SAAMER abilities to define GW momentum fluxes in variable environments, we examine the convergence of mean momentum flux estimates as a function of the analysis interval. For this purpose, vertical profiles of mean zonal and meridional momentum fluxes specified in Case 5 and estimated for 1, 3, and 10 day intervals using the observed meteor distribution for September 2008 are displayed in the top and bottom left three frames of Figure 7. Corresponding normalized momentum flux errors as functions of altitude are shown for each component in the top and bottom right frames of Figure 7, with the RMS error  $R$  defined as the ratio of RMS errors to RMS total momentum flux for each fitting interval as

$$R = \left\{ \sum [\langle u_i'w' \rangle_M - \langle u_i'w' \rangle_S]^2 / N \sum [\langle u_i'w' \rangle_{GW}]^2 \right\}^{1/2}, \quad (4)$$

where  $u_i$  denotes zonal or meridional horizontal velocity, subscripts M and S denote measured and specified mean momentum fluxes in each 1, 3, or 10 day interval, the summation in the numerator is over the intervals comprising the full month,  $N$  is the number of intervals, and the summation in the denominator represents the sum of the temporal averages of the squares of the momentum flux magnitudes for all unique GWs in the motion field, denoted by a subscript GW (thus, the GWs modulated by the semidiurnal tide winds contribute in the denominator).

[23] The momentum flux profiles in Figure 7 exhibit clear convergence of these estimates toward the specified values as the analysis interval increases for all altitudes displayed, with apparent RMS fluctuations of  $\sim 10\text{--}20\text{ m}^2\text{ s}^{-2}$  for 1 day fits,  $\sim 5\text{--}10\text{ m}^2\text{ s}^{-2}$  for 3 day fits, and  $< 5\text{ m}^2\text{ s}^{-2}$  for 10 day fits. Normalized momentum flux errors  $R$  likewise indicate that the observed meteor distribution for September 2008 allows momentum flux estimates that improve as the fitting interval increases, with the larger values suggesting systematic rather than stochastic variations. Despite their source, estimation errors converge to a few percent for 10 day intervals for the zonal momentum flux for which the mean momentum flux is relatively large. Fractional estimation errors are larger, however, for the meridional momentum flux for which the mean is small. Apparent systematic errors of  $\sim 5\text{ m}^2\text{ s}^{-2}$  or less may nevertheless indicate influences of the diurnal variability in meteor detections where diurnal momentum flux variations occur due to GW source variability or tidal filtering.

[24] Given the relatively small momentum flux estimation errors for a superposition of large-amplitude and temporally variable GWs and tides, these results suggest that the same methodology applied to real SAAMER measurements should

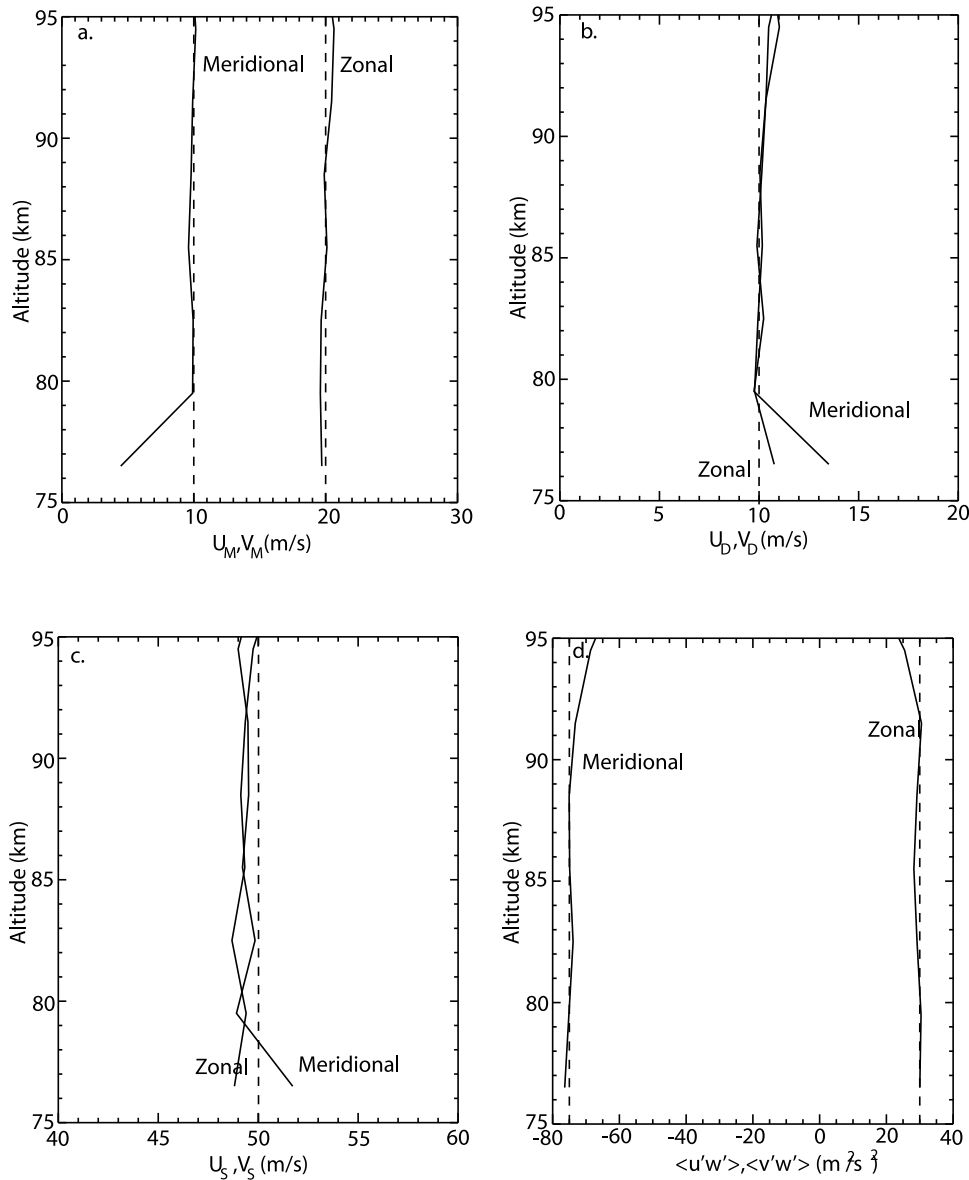


**Figure 4.** As in Figure 3, but for (a) the superposition of the mean winds, (b and c) diurnal and semidiurnal tides, and (d) zonal and meridional propagating GWs in Case 1 and stationary GWs in Case 3 (see Case 4 in Table 1). As in Case 1, recovered momentum fluxes are within  $\sim 2\%$  of specified values, except at the lowest and highest altitudes where meteor detection rates were small.

yield similar accuracies. Nevertheless, we also perform two additional tests of our momentum flux retrieval capabilities for transient GW packets having short periods, variable propagation directions, and random occurrence statistics in Cases 6 and 7 below.

#### 2.2.6. Case 6

[25] Case 6 examines the ability of SAAMER to define GW momentum fluxes for two transient GW packets that occur randomly for 3 and 4 h each day, have periods and 20 and 30 min, zonal and meridional propagation, and both horizontal and vertical phase variations. The GWs are superposed with nominal mean winds and diurnal and semidiurnal tides having realistic amplitudes (see Table 1 for details). The constant mean winds and tidal amplitudes are recovered well for Case 6, as for Cases 1, 4, and 5 above, and are not shown.

GW occurrences and momentum fluxes for one realization of a random distribution are shown in the left and top right frames of Figure 8. GW vertical velocities for the 30 days (with  $w' = 20$  and  $10 \text{ m s}^{-1}$  for the GWs propagating zonally and meridionally, respectively, and successive daily offsets of  $40 \text{ m s}^{-1}$ ) are displayed at top left. The larger vertical velocity fluctuations reveal clustering of the zonal GWs with maxima from  $\sim 3$  to 6 h,  $\sim 13$  to 18 h, and  $\sim 20$  to 21 h of the composite day; the smaller meridional GW vertical velocity fluctuations reveal clustering from  $\sim 8$  to 10 h and  $\sim 16$  to 21 h. Composite day variations of mean zonal and meridional momentum fluxes in the middle and bottom left frames reveal maxima centered on these same time intervals and suggesting that our analysis reasonably describes the composite day variations for the prescribed random GW distribution. Mean momen-

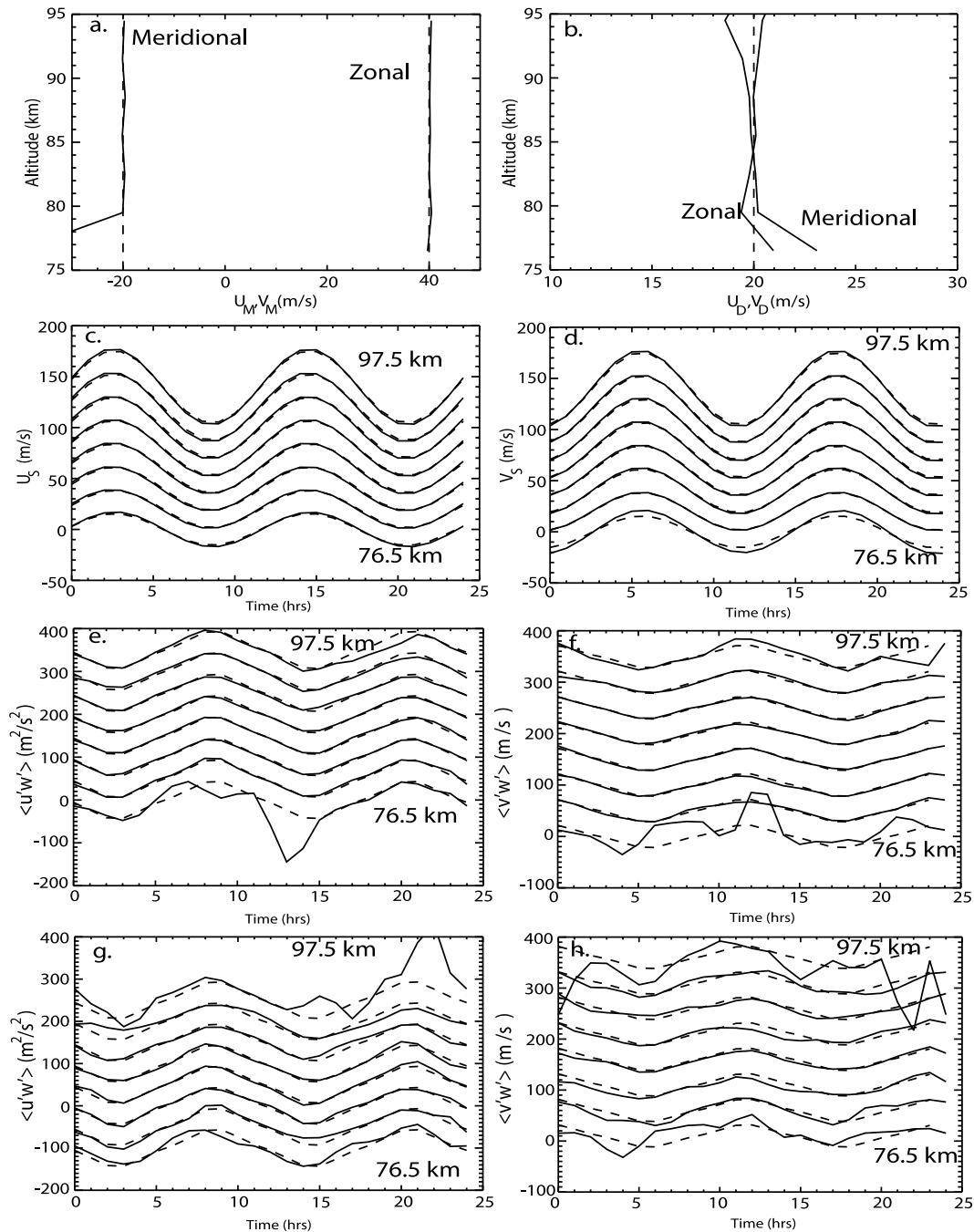


**Figure 5.** (a) Zonal and meridional 30 day mean winds, (b) diurnal tide amplitudes, and (c and d) composite day hourly semidiurnal tides for Case 5. (e and f) Zonal and meridional composite day hourly GW momentum fluxes for those GWs modulated by the semidiurnal tide. (g and h) Zonal and meridional composite day hourly GW momentum fluxes for the superposition of zonal and meridional stationary GWs and those GWs modulated by the semidiurnal tide. Specified and recovered fields are shown with dashed and solid lines, offsets between successive 3 km altitudes are  $20 \text{ m s}^{-1}$  for the semidiurnal tide and  $50 \text{ m}^2 \text{ s}^{-2}$  for the GW momentum fluxes. Altitudes range from 76.5 to 97.5 in each frame. Small meteor detection rates limited measurement accuracies at the highest and lowest altitudes.

tum flux profiles shown for these zonal and meridional GW distributions at upper right reveal an  $\sim 5\%$ – $10\%$  average underestimate of the total momentum flux in each component for this test.

[26] To further assess the robustness of these mean estimates, we also performed a series of additional mean

momentum flux estimates for the same GW parameters, but with different random GW occurrences. These results are shown for 10 such estimates in the bottom right frames of Figure 8 and reveal that they cluster about the specified mean momentum fluxes, but with an apparent average underestimate of each by  $\sim 5\%$ – $10\%$  at altitudes from 79.5 to 91.5 km,

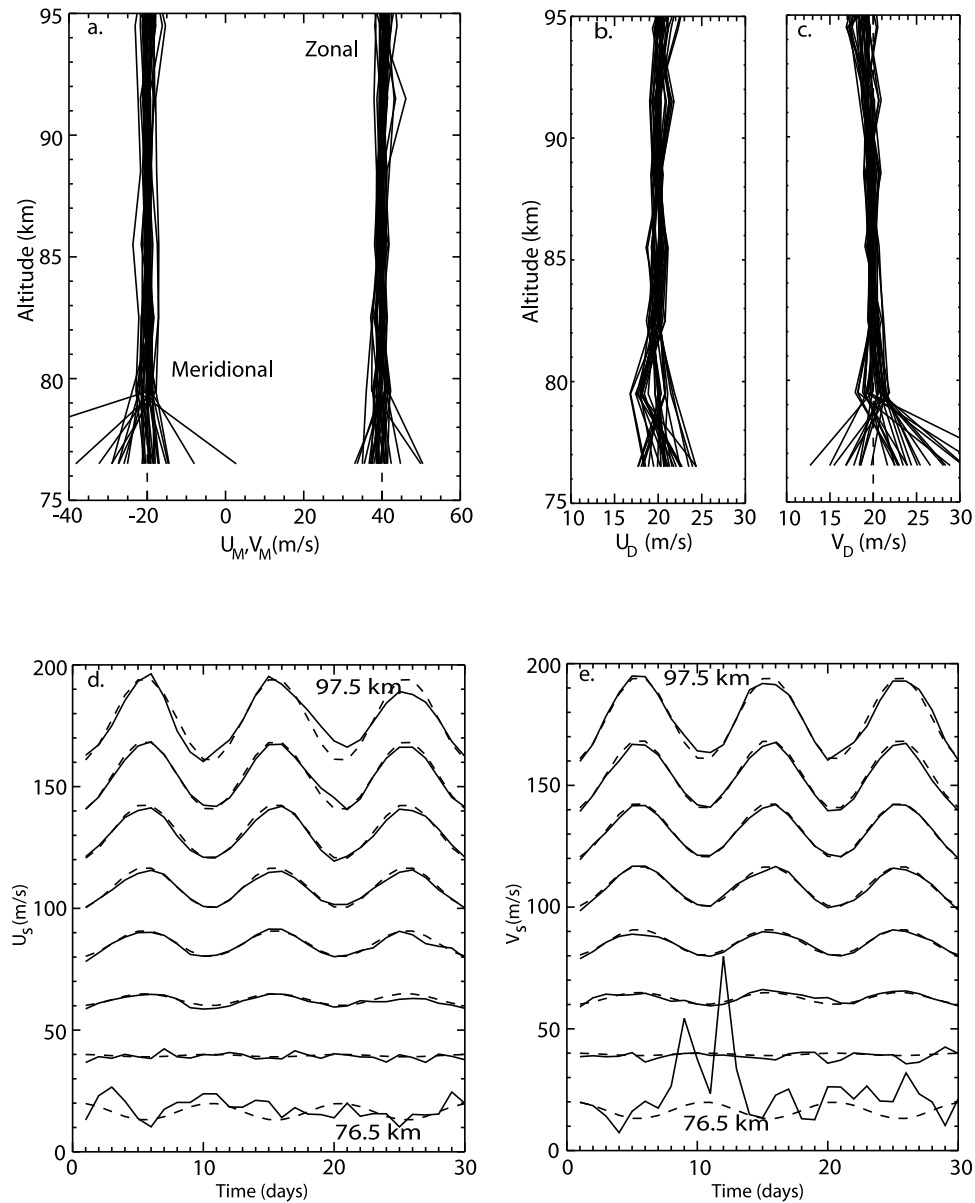


**Figure 6.** (a) Daily zonal and meridional mean winds, (b and c) diurnal tide amplitudes, and (d and e) semi-diurnal tide amplitudes for 1 day fits (solid) to the specified motion field in Case 5 (dashed) assuming the meteor distribution observed for September 2008. Successive profiles in Figures 6d and 6e are offset by  $20 \text{ m s}^{-1}$ . Departures of the recovered winds and amplitudes from those specified are  $\sim$ a few  $\text{m s}^{-1}$  in each case, except at the lowest and highest altitudes (76.5 and 97.5 km), suggesting that SAAMER reliably defines the large-scale motion field on a daily basis where meteor detection rates are relatively high.

with slightly greater uncertainties at the lowest and highest altitudes where meteor counts are smallest. Thus, there are apparently systematic and statistical uncertainties in GW momentum flux estimates accompanying discrete GW packets that collectively vary from  $\sim 20\%$  underestimates to  $\sim 10\%$  overestimates in our monthly means estimates. These results imply somewhat greater uncertainty in momentum flux assessments with SAAMER than suggested by Cases 1–5 with fixed (or slowly varying) GW characteristics throughout a 30 day interval.

#### 2.2.7. Case 7

[27] Case 7 closely parallels Case 6, with the same mean and tidal winds, but for GW packets having durations of only

1 and 2 h, periods of 15 and 20 min, horizontal and vertical phase variations, and propagation toward the NE and SE. In this case, the GWs having a 1 h duration occur 4 times each day, propagate to the NE, and contribute zonal and meridional momentum fluxes of  $50 \text{ m}^2 \text{ s}^{-2}$  each day, whereas the GWs having a 2 h duration occur 2 times each day, propagate to the SE, and contribute zonal and meridional momentum fluxes of  $50$  and  $-50 \text{ m}^2 \text{ s}^{-2}$ , respectively, each day. Thus the specified composite day momentum fluxes are anticipated to be  $75$  and  $-25 \text{ m}^2 \text{ s}^{-2}$ , respectively.

[28] As above, results for Case 7 are shown in Figure 9 for a typical random distribution of GWs and for a series of 10 such distributions in order to assess the SAAMER ability to

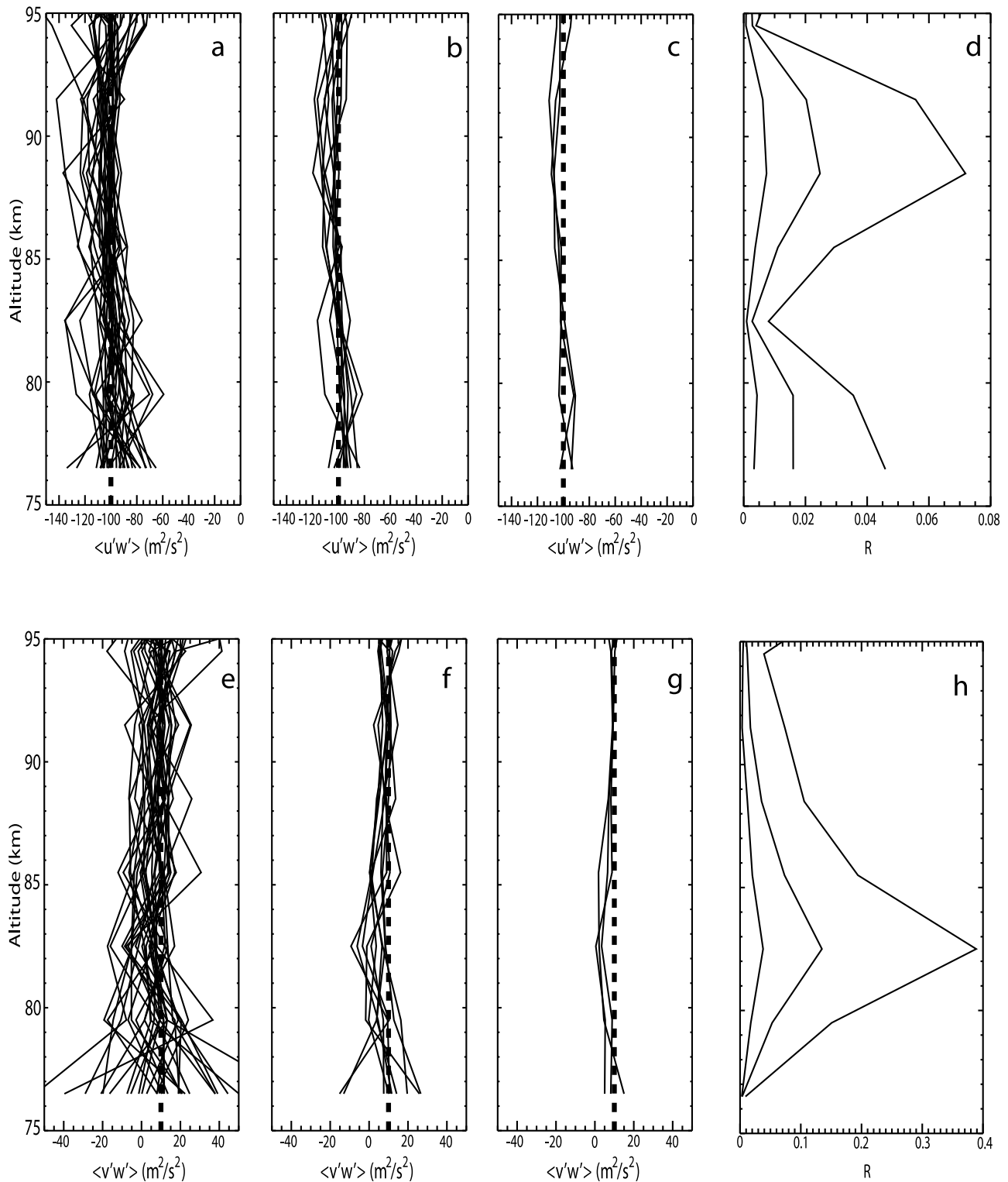


**Figure 7.** Vertical profiles of (a, b, and c) zonal and (e, f, and g) meridional momentum flux specified (dashed lines) and recovered (solid lines) for 1, 3, and 10 day intervals throughout the 30 day period for Case 5 with the meteor distribution observed during September 2008. Note that momentum flux estimates converge to the correct mean values for the stationary GWs as the fitting interval lengthens, even in the presence of assumed comparable or larger semidiurnal momentum flux modulations of zonally and meridionally propagating GWs. (d and h) The ratio  $R$  for zonal and meridional 1, 3, and 10 day fits using the September 2008 meteor occurrences for the Case 5 specified fields. Note that momentum flux errors appear to reduce to a few percent of the total momentum flux in each component as the fitting interval increases toward a month.

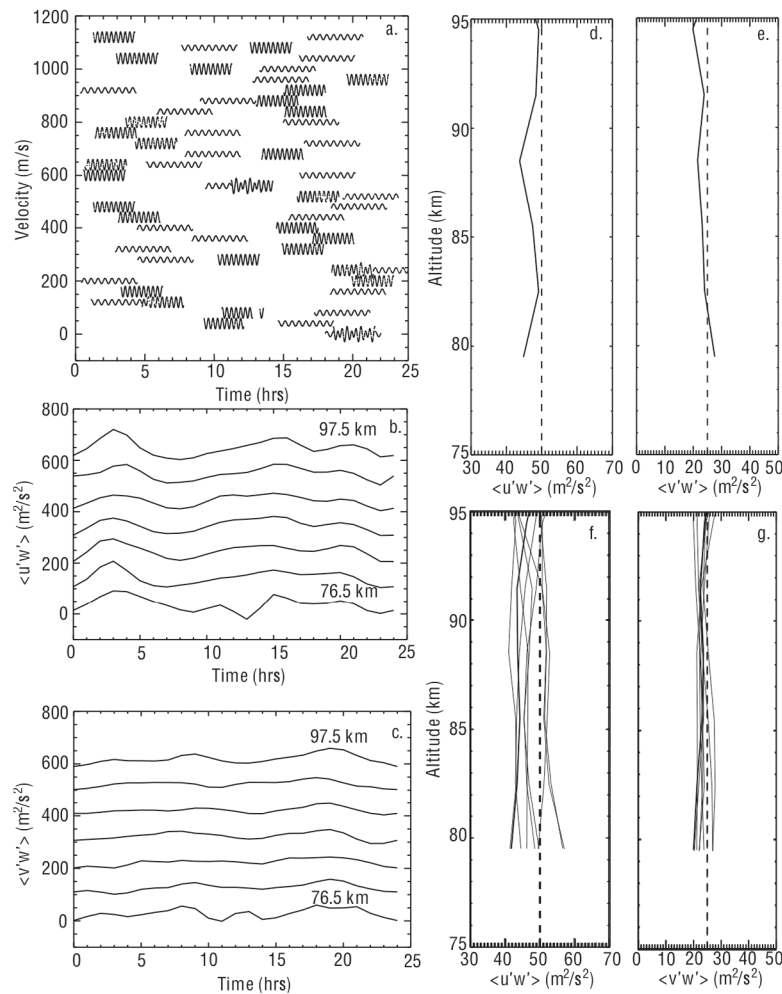


**Figure 8.** (a) Case 6 vertical velocities showing the occurrence of random superposed GWs throughout the assumed test interval of September 2008. Vertical velocities of 20 and 10  $\text{m s}^{-1}$  indicate occurrences of GWs having 3 and 4 h durations and propagating in the zonal and meridional directions, respectively. (b and c) Diurnal variations throughout the composite day and (d and e) monthly mean profiles of the zonal and meridional momentum fluxes inferred for September 2008 meteor distributions based on the GW occurrences shown in frame a. (f and g) Monthly mean momentum flux profiles for 10 random GW distributions exhibit the range of variability observed in Case 6.

describe the mean momentum fluxes for shorter-duration and shorter-period GWs. Results in Figure 9 are very consistent with those described for Case 6. Relative maxima in the GW occurrence are again seen clearly in the composite day diurnal momentum flux variability, with typical underestimates of the specified mean zonal and meridional momentum fluxes of  $\sim 5\%$ – $10\%$ , apart from the larger departure at 79.5 km in the meridional component. Similar statistics are also seen in the summary of the 10 random GW distributions shown in Figure 9 at bottom right, but now for GWs propagating obliquely and contributing differently to the zonal and meridional fluxes. As above, zonal momentum flux estimates vary from  $\sim 10\%$  underestimates to  $\sim 5\%$  overestimates (apart from individual outliers at the lowest and highest altitudes), while meridional momentum fluxes vary from  $\sim 25\%$  underestimates to  $\sim 10\%$  overestimates (apart from outliers now at the highest altitude).

[29] We expect that the somewhat greater uncertainties seen in the meridional momentum flux estimates in Case 7

arise from offsetting contributions of orthogonally propagating GWs.

[30] Thus, even in highly modulated and complex superpositions of mean, tidal, and GW motions, our tests suggest that SAAMER retains an ability to define mean winds, tidal amplitudes, and GW momentum fluxes, their spatial and temporal variability, and correlations between these various motions that appear in monthly-averaged, multiday, or composite day estimates with accuracies that we hope will be useful in assessments using real SAAMER data. Such applications for several test months at various seasons are described below.

### 3. Monthly Mean and Composite-Day Winds, Tides, and GW Momentum Fluxes

[31] Given the apparent ability of SAAMER meteor distributions to recover specified mean winds, tides, and GW momentum fluxes for simple and more complex and variable

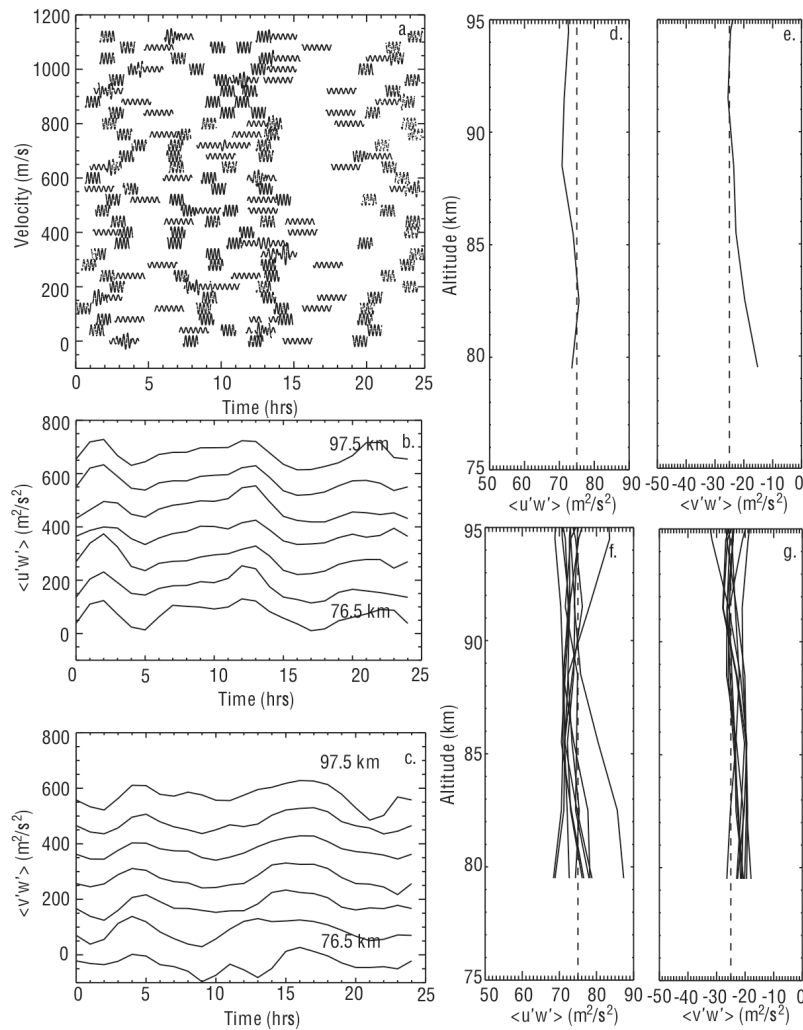


**Figure 9.** As in Figure 8, but for Case 7.

motion fields (and stationary and propagating GWs), we now apply the same methodology to real SAAMER measurements during June, September, and November 2008 and March and June 2009, as approximations to solstice and equinox conditions during the first  $\sim 17$  months of operations. These assessments were not possible during December 2008 and September 2009 because of incomplete monthly measurements due to antenna connection failures or system maintenance. Results of our assessments for these 5 months are shown in Figures 10 and 12–15 and discussed separately below.

### 3.1. June 2008 Data

[32] Mean winds, tidal amplitudes, and GW momentum fluxes obtained with SAAMER for June 2008 are displayed in Figure 10. Vertical profiles of monthly-mean zonal and meridional winds, diurnal and semidiurnal tidal amplitudes, and GW momentum fluxes are shown (left to right) in the top frames. Daily zonal and meridional (solid and dashed lines) diurnal and semidiurnal (left and right) tidal amplitudes are shown at 3 km altitude intervals in the second frames. Hourly mean zonal and meridional (left and right) winds and GW momentum fluxes for a composite day for all June data are

shown at 3 km altitude intervals in the third and fourth frames. In these plots and those presented for other months below, we show vertical profiles of mean winds and tidal amplitudes from 79.5 to 97.5 km and GW momentum fluxes from 79.5 to 94.5 km. Daily tidal amplitudes and hourly winds for a composite day are shown from 79.5 to 97.5 km, and hourly momentum fluxes for a composite day are shown from 79.5 to 94.5 km. The smaller altitude ranges displayed for the various fields are due to our varying confidence in the wind, tidal amplitude, and GW momentum flux estimates based on meteor detection rate variations with altitude and the varying influences of superposed motions as functions of altitude. Mean winds can be reliably estimated at altitudes between  $\sim 75$  and 100 km because they are not biased by diurnal or azimuthal variations in meteor detections. Tidal amplitudes can likewise be estimated well at these same altitudes, except where both tidal amplitudes and meteor detections are small. GW momentum fluxes appear to be reliable over the smallest altitude range, as suggested by the test fields in Case 5 displayed in Figure 5, where meteor detections appear marginal below  $\sim 79.5$  km and large tidal variations combine with decreasing meteor detections to increase uncertainties above  $\sim 95$  km.

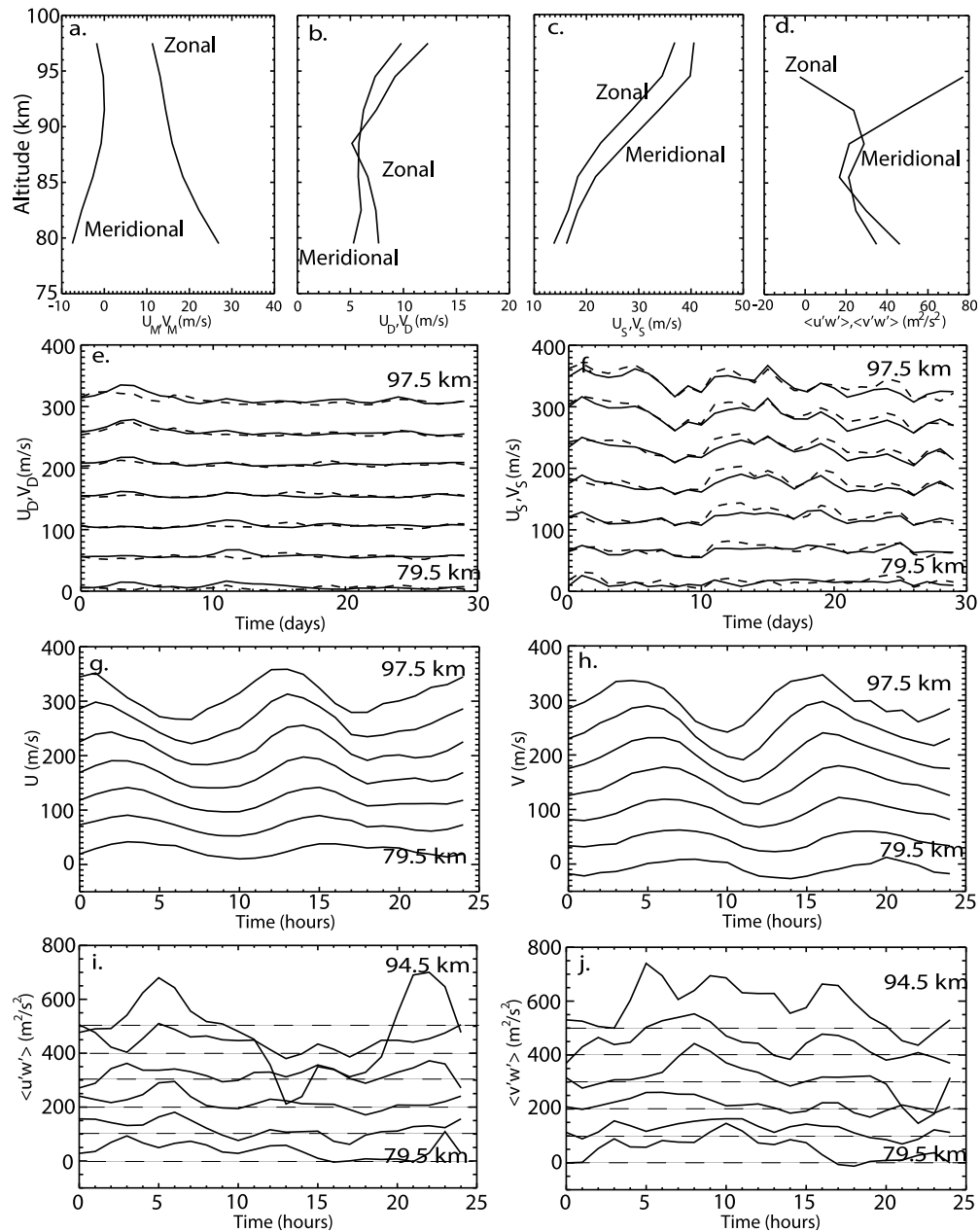


**Figure 10.** (a) June 2008 monthly mean zonal and meridional winds, (b and c) diurnal and semidiurnal tide amplitudes, and (d) GW momentum fluxes. Daily zonal and meridional (solid and dashed) (e) diurnal and (f) semidiurnal tide amplitudes at altitudes from 79.5 to 97.5 km at 3 km intervals. Hourly mean (g) zonal and (h) meridional winds for a composite day at altitudes from 79.5 to 97.5 km, and hourly mean (i) zonal and (j) meridional GW momentum fluxes for a composite day at altitudes from 79.5 to 94.5 km. Offsets of successive altitudes are  $50 \text{ m s}^{-1}$  in frames e–h and  $100 \text{ m}^2 \text{ s}^{-2}$  in frames i–j.

[33] The June 2008 mean zonal wind is seen to decrease from  $\sim 27 \text{ m s}^{-1}$  at 79.5 km to  $\sim 10 \text{ m s}^{-1}$  at 97.5 km above the winter eastward jet at this latitude, with magnitudes slightly stronger than seen in the mean winds for June (see the second frame of Figure 11), with departures likely due to planetary wave (PW) influences discussed by F10. The mean meridional wind increases from  $\sim -7 \text{ m s}^{-1}$  at 79.5 km to  $\sim 0 \text{ m s}^{-1}$  at  $\sim 90$  km and above, again suggesting PW influences discussed by F10.

[34] Mean diurnal tidal amplitudes are generally small,  $\sim 10 \text{ m s}^{-1}$  or less at all altitudes, while mean semidiurnal

amplitudes increase from  $\sim 15 \text{ m s}^{-1}$  at 79.5 km to  $\sim 35$  to  $40 \text{ m s}^{-1}$  at 97.5 km. Tidal amplitude estimates are slightly larger here than reported by F10 because that study employed a monthly fit whereas this study computes a monthly mean from the average of daily estimates employing the S transform (see below). The two estimates typically agree within a few  $\text{m s}^{-1}$ , with the S transform results being somewhat larger because the mean does not account for phase variations between daily estimates.

[35] GW momentum flux profiles shown at top right in Figure 10 exhibit significantly larger values than seen in any

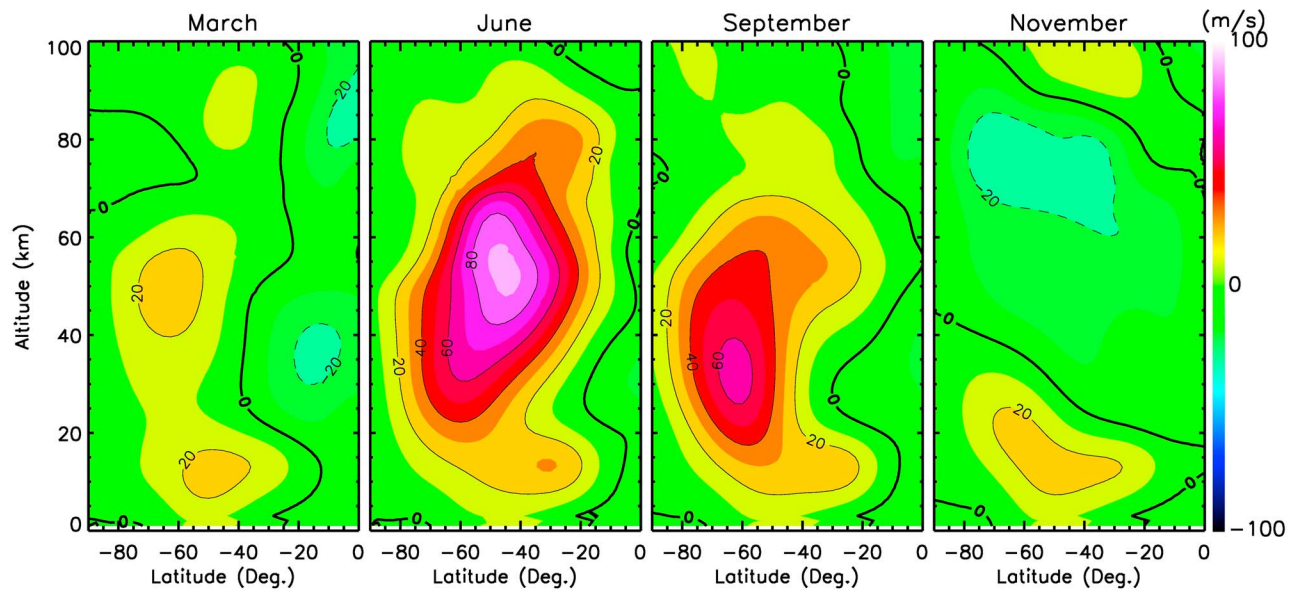


**Figure 11.** Cross sections of monthly zonal winds from 0 to 90°S and 0 to 100 km for March, June, September, and November from model and observational data (images from <http://www.uni-leipzig.de/~jacobi/intas03>, courtesy of H. Iimura and Ch. Jacobi). The assimilated fields employ UKMO data from 0–55 km, Global Empirical Wind Model data [Portnyagin *et al.*, 2004] from 70–100 km, and numerical model results from 55–70 km [see Jacobi *et al.*, 2009].

monthly mean at any other site, even at the intermediate altitudes from 82.5 to 91.5 km where meteor counts suggest the highest confidence. These profiles were also smoothed with a 1-2-1 triangular filter to increase confidence in the larger-scale trends. The zonal momentum flux exhibits a decrease from  $\sim 35 \text{ m}^2 \text{ s}^{-2}$  at 79.5 km to smaller values at higher altitudes. The meridional momentum flux, however, remains between  $\sim 20$  and  $50 \text{ m}^2 \text{ s}^{-2}$  at altitudes of 91.5 km and below, with a reduction with altitude up to  $\sim 85$  km and an increase with altitude above. These magnitudes are smaller than those of the test fields discussed above that were assessed reasonably accurately with real SAAMER meteor distributions, so we have confidence in these estimates, at least at intermediate altitudes, with the caveat that random distributions of discrete GW packets appear to yield an underestimate of the momentum flux by  $\sim 5\%$ – $10\%$ , on average.

[36] The constant or decreasing zonal momentum flux with altitude implies an eastward (local) body force that is different from what we expect at these altitudes, where the zonal-mean momentum flux is typically negative in winter and its divergence yields a body force expected to reverse (or reduce) the zonal-mean zonal wind in the MLT. The large meridional momentum flux likewise differs significantly from the much smaller mean values at other sites, suggesting a local GW source yielding strong northward propagation over SAAMER.

[37] These results might be expected, however, given the location of SAAMER within the northern edge of the region spanning the southern Andes, the Drake Passage, and the Antarctic Peninsula [McLanress *et al.*, 2000; Jiang *et al.*, 2002, 2006; Wu and Jiang, 2002; Wu, 2004; Ern *et al.*, 2004] which exhibits one of the, if not the, largest enhancement of GW amplitudes and implied momentum fluxes extending into the MLT under winter conditions of any site on Earth. These enhancements are apparently due to very

strong GW excitation by sources in the lower atmosphere. Indeed, the center of this “hot spot” of dynamical activity is over, and in the lee of, the Drake Passage, despite the occurrence of major topography well to the north and south, and the lack of significant topography within this region itself. This suggests that other sources, especially storm systems and jet stream imbalances and instabilities (with mean eastward winds of  $\sim 90 \text{ m s}^{-1}$  at  $\sim 50$  km (see Figure 11, second frame), may be playing a major role in GW excitation in this region. If so, GW phase speeds arising from these sources should be expected to be large, with GWs propagating eastward with high zonal phase speeds and meridionally away from the Drake Passage with phase speeds depending on the source character. Both of these expectations appear to be consistent with observations of large and positive zonal and meridional GW momentum fluxes over SAAMER in June 2008.

[38] Daily tidal amplitudes (second frames of Figure 10) reveal that the diurnal tide typically remained small throughout June 2008, with several  $\sim 2$  day enhancements having amplitude increases of  $\sim 20 \text{ m s}^{-1}$  that spanned several altitude ranges. Semidiurnal amplitudes were typically much larger, especially at higher altitudes, with the meridional amplitude typically larger than the zonal, both components exhibiting significant variability on  $\sim 4$  to 15 day periods, and temporal amplitude modulations as large as  $\sim 30$ – $50 \text{ m s}^{-1}$  at intermediate and higher altitudes.

[39] Zonal and meridional wind variations throughout a composite day (third frames in Figure 10) at 3 km altitude intervals exhibit primarily semidiurnal tidal winds, with apparent quadrature between the zonal and meridional components, the mean growth with increasing altitude discussed above, and a clear phase descent with time. Corresponding variations of GW momentum flux throughout a composite

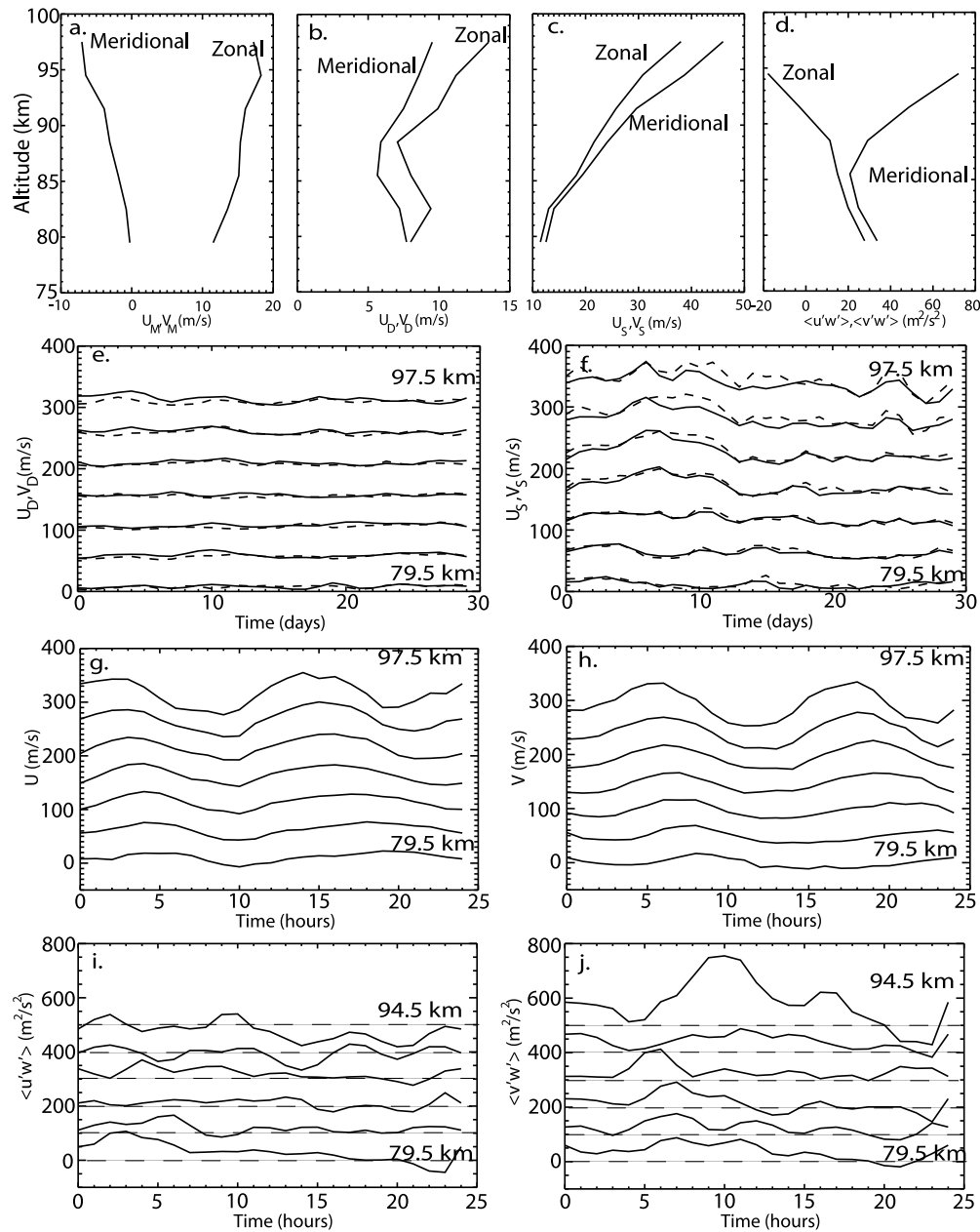


**Figure 12.** As in Figure 10, but for September 2008.

day (bottom frames) exhibit significantly greater temporal variability (and greater uncertainties), but with the lower-frequency variations reasonably consistent between adjacent altitudes (except at the highest and lowest altitudes). Note, in particular, the general tendency for larger (positive) momentum fluxes in both zonal and meridional components early in the diurnal cycle ( $\sim 5$  LT) and smaller momentum fluxes later in the diurnal cycle ( $\sim 20$  LT), suggestive of a diurnal rather than a semidiurnal modulation of the momentum flux in each component. We also note that adjacent altitudes provide independent estimates of the momentum fluxes (and all other assessed quantities), implying some confidence in these estimates. Hourly estimates at intermediate altitudes occasionally approach  $\sim 150 \text{ m}^2 \text{ s}^{-2}$ , with magnitudes as large as  $\sim 200 \text{ m}^2 \text{ s}^{-2}$  at 94.5 km, where uncertainties are larger due to lower meteor detections.

Only the diurnal cycle in zonal momentum flux at 94.5 km appears inconsistent in magnitude with other altitudes for the  $\sim$ diurnal variations. The diurnal consistency of these data where meteor counts are high and tidal amplitudes are smaller provide additional confidence in the monthly-mean momentum flux profiles at top right in Figure 10, at least at altitudes of 82.5–91.5 km (with the above caveat about apparent underestimates for transient GW packets of  $\sim 5\%$ – $10\%$ ). Additional confidence is acquired by comparing these measurements with those during June 2009 discussed below, which exhibit very similar mean and composite day diurnal momentum flux variations.

### 3.2. September 2008 Data

[40] Mean winds, tidal amplitudes, and GW momentum fluxes obtained with SAAMER for September 2008 are

displayed in the same format discussed above in Figure 12. September 2008 mean zonal winds are smaller than during June and consistent with an equinox state without a strong mesospheric jet (see the third frame of Figure 11), though the strong stratospheric jet may still play an important role in GW forcing during this period. Mean meridional winds are comparable to June, though now with the opposite trend in altitude, again likely reflecting PW influences discussed by F10. Mean diurnal and semidiurnal tidal amplitudes are also very similar to those during June 2008, with diurnal amplitudes  $\sim 5\text{--}13\text{ m s}^{-1}$  and the zonal component somewhat larger, and semidiurnal amplitudes now increasing from  $\sim 12\text{ m s}^{-1}$  at 79.5 km to  $\sim 38$  to  $46\text{ m s}^{-1}$  at 97.5 km, again with the meridional component larger at all altitudes. Tidal amplitudes also exhibit similar daily variations to those seen in June 2008, with weaker amplitude variations that are coherent over several altitudes in the diurnal tide, and coherent amplitude modulations again as large as  $\sim 50\text{ m s}^{-1}$  in the semidiurnal tide. Diurnal wind variations throughout the September composite day closely resemble those for June 2008. Specific differences include (1) semidiurnal tide phases that are delayed by  $\sim 2\text{ h}$  compared to June 2008 and (2) an apparent faster semidiurnal phase descent in September 2008 than during June 2008.

[41] GW momentum flux profiles shown at top right in Figure 12 are very similar to those for June 2008. Mean zonal fluxes during September decrease nearly uniformly from  $\sim 28\text{ m}^2\text{ s}^{-2}$  at 79.5 km and  $\sim 20\text{ m}^2\text{ s}^{-2}$  at 82.5 km (where meteor counts are  $\sim 2$  times higher) to  $\sim 18\text{ m}^2\text{ s}^{-2}$  at 94.5 km, with mean meridional fluxes  $\sim 33$  and  $25\text{ m}^2\text{ s}^{-2}$  at 79.5 and 82.5 km, decreasing to  $\sim 20\text{ m}^2\text{ s}^{-2}$  at  $\sim 85$  km, and increasing above to  $\sim 72\text{ m}^2\text{ s}^{-2}$  at 94.5 km. As above, our extensive tests of the SAAMER ability to define momentum fluxes described in section 2 give us confidence in these results (within  $\sim 10\%$ – $20\%$ ), except where estimates do not exhibit coherence between adjacent altitudes. Even excluding the mean momentum flux estimates at 94.5 km (where meteor counts are high, but tidal modulation is very strong), these results suggest that strong forcing of GWs that penetrate into the MLT continues within the “hot spot” centered over the Drake Passage into September. Additional support for this is provided by the continuing strength of the stratospheric jet, with even stronger winds at  $\sim 30$  km in September than in June (see Figure 11) and high GW variances seen in MLS data in the upper stratosphere and mesosphere often extending into September [see *Wu and Jiang, 2002; Jiang et al., 2006*].

[42] Variations of GW momentum fluxes throughout a September 2008 composite day (bottom frames of Figure 12) closely resemble those described for June 2008. At intermediate altitudes (excluding 94.5 km), these again exhibit decreasing zonal and meridional momentum fluxes with time from  $\sim 5$  to 20 LT and maximum values of  $\sim 100\text{ m}^2\text{ s}^{-2}$ , thus also suggestive of a diurnal modulation of momentum fluxes due to either GW sources or filtering conditions.

### 3.3. November 2008 Data

[43] Mean winds, tidal amplitudes, and GW momentum fluxes obtained during November 2008 are displayed in the same format discussed above in Figure 13. Mean zonal winds differ greatly from those seen in June and September 2008, with a westward maximum of  $\sim 43\text{ m s}^{-1}$  at  $\sim 80$  km shifting to

eastward winds above  $\sim 91$  km. Indeed, these winds are about twice those expected in the UKMO analysis at lower altitudes (see the right frame of Figure 11), though the transition to eastward winds seems to agree well. Mean meridional winds are  $\sim 0$  or very weakly positive during this period. The mean diurnal tide remains small and is nearly uniform in altitude during November, with component amplitudes of  $\sim 6\text{--}9\text{ m s}^{-1}$ . Mean semidiurnal amplitudes are much smaller during November than June or September, with minimum amplitudes of  $\sim 10\text{ m s}^{-1}$  at lower altitudes increasing to  $\sim 20\text{--}23\text{ m s}^{-1}$  at 91.5 km and above. Tidal amplitudes exhibit daily variability in November that is smaller than seen in June or September 2008 because of the smaller mean amplitudes, but with similar periodicities. Semidiurnal tidal phases are advanced in LT compared to both June and September 2008 data at higher altitudes, with differences of  $\sim 2\text{--}4\text{ h}$ , respectively. The November semidiurnal tide also exhibits smaller phase variations with altitude, suggesting a larger vertical wavelength at this time.

[44] GW momentum flux profiles for November 2008 shown at top right in Figure 13 are similar in the zonal component but differ dramatically from those obtained during June and September 2008 in the meridional component. Mean zonal momentum fluxes vary from  $\sim 10$  to  $22\text{ m}^2\text{ s}^{-2}$  from 79.5 km to 94.5 km, in approximate antiphase with the mean zonal wind during November, as seen in previous MLT measurements at a number of locations [*Vincent and Reid, 1983; Fritts and Vincent, 1987; Fritts and Yuan, 1989; Wang and Fritts, 1990; Tsuda et al., 1990; Nakamura et al., 1993*]. Mean meridional momentum fluxes for November 2008 also differ dramatically from June and September 2008 measurements and are large and negative,  $\sim -38\text{ m}^2\text{ s}^{-2}$  at 91.5 km and increase to  $\sim 10\text{ m}^2\text{ s}^{-2}$  from 91.5 km, with larger but less reliable magnitudes at lower and higher altitudes. We also note that the temporal variability of the estimated momentum fluxes at the lowest and highest altitudes displayed are especially high during November (79.5, 82.5, and 94.5 km in this case), suggesting less confidence in the November estimates at these altitudes. This is especially true given the lack of continuity between adjacent altitudes that we expect for the large vertical wavelength GWs required to account for large fluxes. Where there is greater continuity in altitude (from 85.5 to 91.5 km), mean zonal and meridional momentum fluxes are still significant, and our evaluation of SAAMER momentum flux measurement capabilities above suggests that these estimates should be reasonable within the  $\sim 10\%$ – $20\%$  uncertainties estimated above. Whereas large and positive mean meridional momentum fluxes during June and September suggest strong GW sources within the “hot spot” centered over the Drake Passage, negative (positive) mean meridional (zonal) momentum fluxes during November suggest GW sources primarily to the north and west of SAAMER, and these GWs apparently dissipate strongly over the observed altitude interval.

[45] A possible source for some of these motions is the deep tropical convection over South America during austral summer, which regularly extends to  $\sim 30^\circ\text{S}\text{--}35^\circ\text{S}$ . Indeed, relatively large-scale GWs from deep convection have been shown by *Vadas and Fritts [2004, 2009]* to readily achieve large amplitudes and penetrate into the MLT and above. At distances of  $\sim 2000$  km from the GW sources, however,

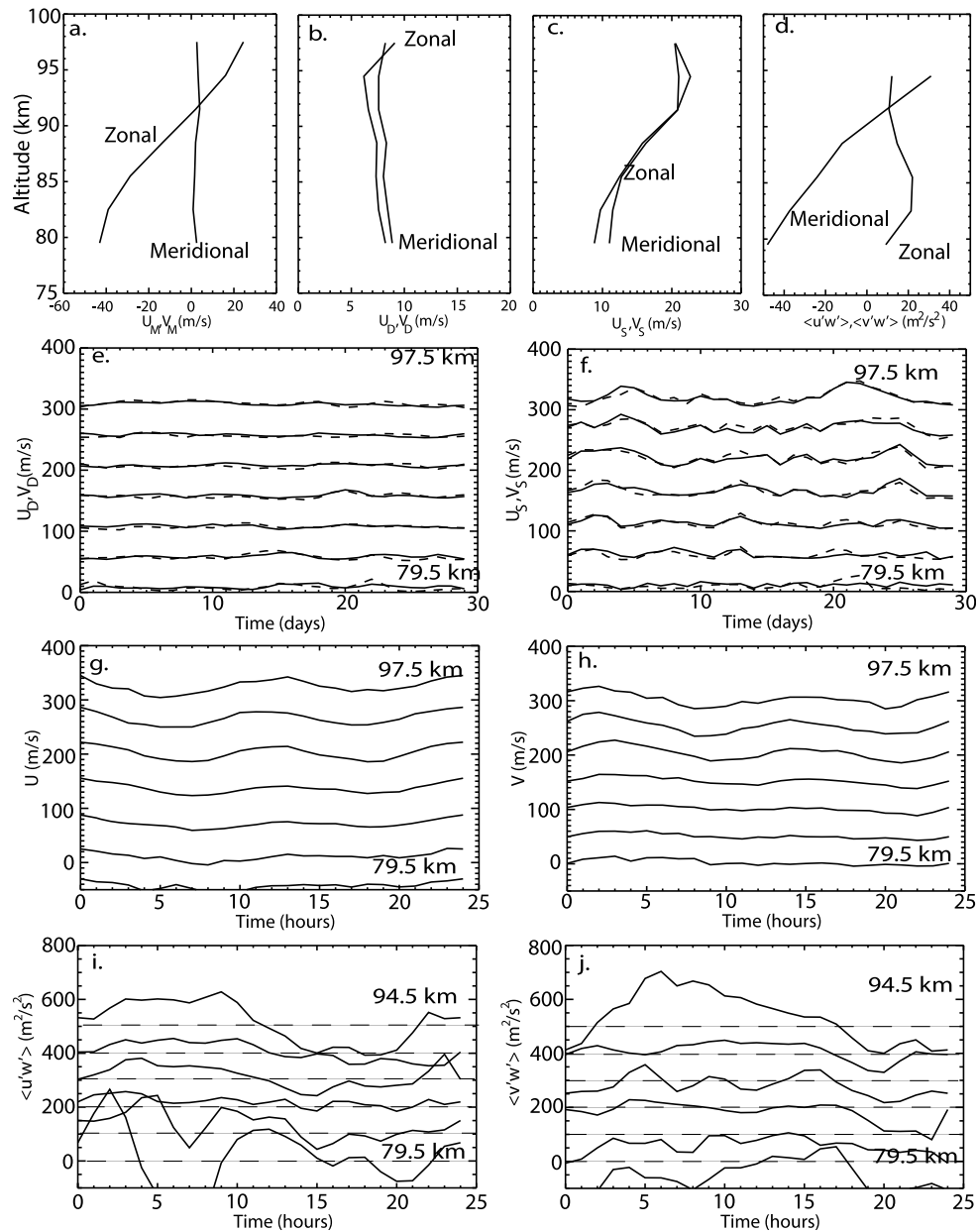


**Figure 13.** As in Figure 10, but for November 2008.

momentum fluxes would typically be smaller than observed (due to a need for small phase slopes and vertical motions, unless these GWs are strongly refracted by mean and tidal winds), so a more local, but as yet unidentified, source appears more likely. Finally, variations of GW momentum fluxes throughout a composite day for November 2008 (bottom frames of Figure 13) exhibit diurnal variability somewhat similar to that seen during June and September, though with smaller apparent amplitudes, especially in the zonal component at intermediate altitudes. While no clear correlation is apparent with the tidal winds that are expected to filter GWs propagating vertically, such variations may provide clues to source or filtering influences when they are diagnosed more completely in the future.

### 3.4. March 2009 Data

[46] Mean winds, tidal amplitudes, and GW momentum fluxes obtained with SAAMER during March 2009 are displayed in the same format discussed above in Figure 14. Mean zonal winds exhibit initial formation of a new eastward winter jet, with a maximum of  $\sim 16 \text{ m s}^{-1}$  at  $\sim 85 \text{ km}$  (appearing  $\sim$  a month earlier than in the UKMO data, see left frame of Figure 11), while mean meridional winds are nearly identical to those seen during June 2008. Diurnal tidal amplitudes most closely resemble those seen during November 2008, with magnitudes of  $\sim 6\text{--}10 \text{ m s}^{-1}$  at low and intermediate altitudes and smaller values above. Semidiurnal tidal amplitudes are slightly larger than seen in November 2008, but also smaller than seen in June and September 2008 by  $\sim 5\text{--}15 \text{ m s}^{-1}$  at the highest altitudes, with amplitudes increas-

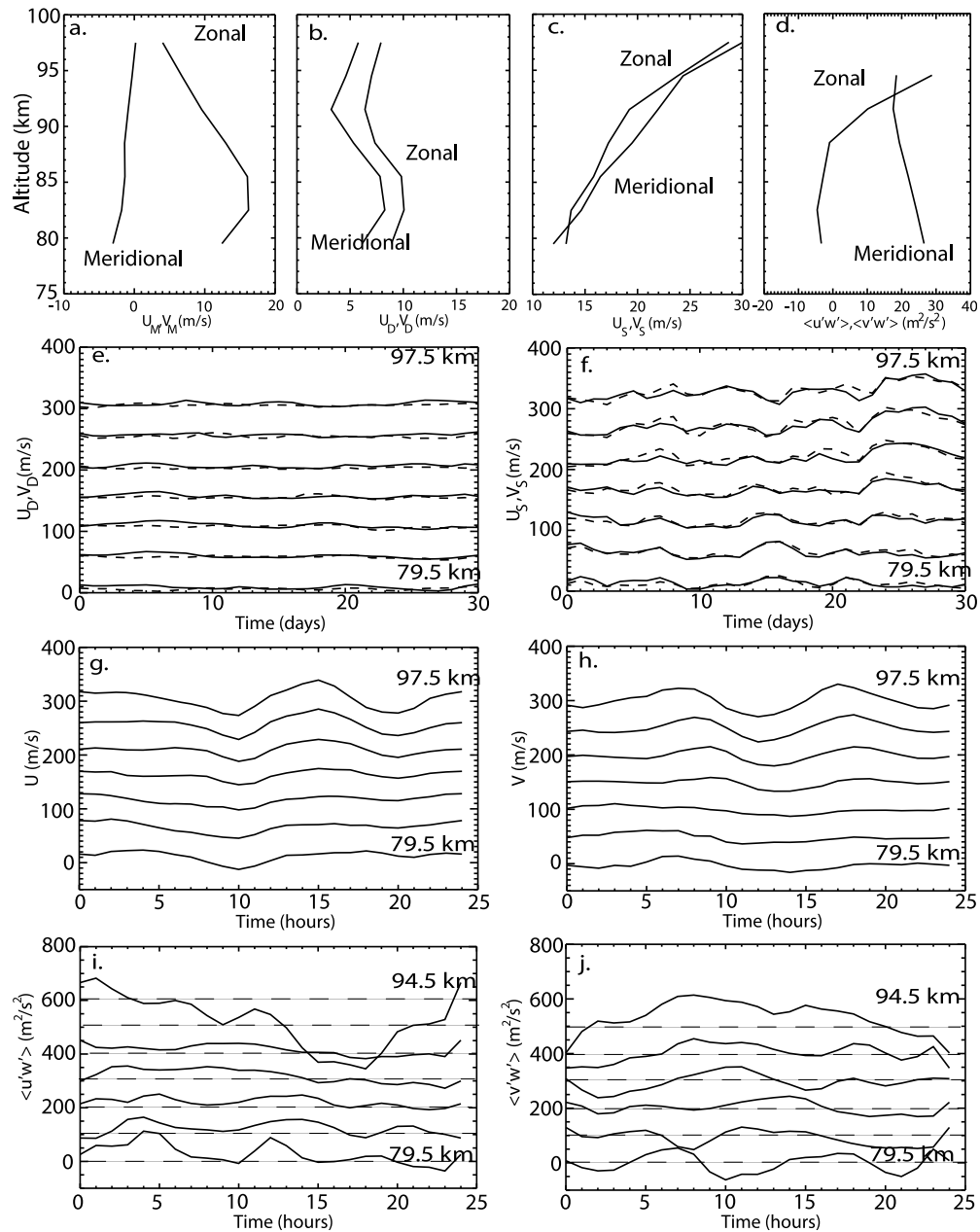


**Figure 14.** As in Figure 10, but for March 2009.

ing from  $\sim 13 \text{ m s}^{-1}$  at 79.5 km to  $\sim 30 \text{ m s}^{-1}$  at 97.5 km. Daily tidal variability appears to be very similar to that discussed above, with the same periodicities and primarily semidiurnal amplitude modulations that appear more similar to the larger variations seen in June and September 2008 than the smaller variations seen in November 2008 (where mean amplitudes were smaller). Referring to the composite day wind variations, we see that semidiurnal tidal phases are most similar to those during September 2008, and lag those during June and November 2008 by  $\sim 2\text{--}4$  h or more.

[47] GW momentum flux profiles for March 2009 shown at top right in Figure 14 are different from those discussed above in several respects. First, zonal momentum fluxes are negative for the first time at lower altitudes, with the most negative value of  $\sim -5 \text{ m}^2 \text{ s}^{-2}$  at 82.5 km, approaching 0 at 88.5 km

and only becoming  $\sim 10 \text{ m}^2 \text{ s}^{-2}$  at 91.5 km. As in November 2008, we observe an anticorrelation between the zonal mean wind and momentum flux, as previously seen at other sites, but with larger mean momentum fluxes than observed elsewhere during both November 2008 and March 2009. Mean meridional momentum fluxes are seen to also be anticorrelated with the mean meridional wind during March 2009, with magnitudes decreasing from  $\sim 25 \text{ m}^2 \text{ s}^{-2}$  from 79.5 to 82.5 km to  $\sim 20 \text{ m}^2 \text{ s}^{-2}$  at 91.5 km and above. Indeed, both November 2008 and March 2009 SAAMER measurements suggest more typical filtering of GWs by mean and large-scale winds than seen during June and September 2008 and are consistent with the observed small stratospheric GW variances and apparent lack of strong GW forcing over the Drake Passage and southern South America at

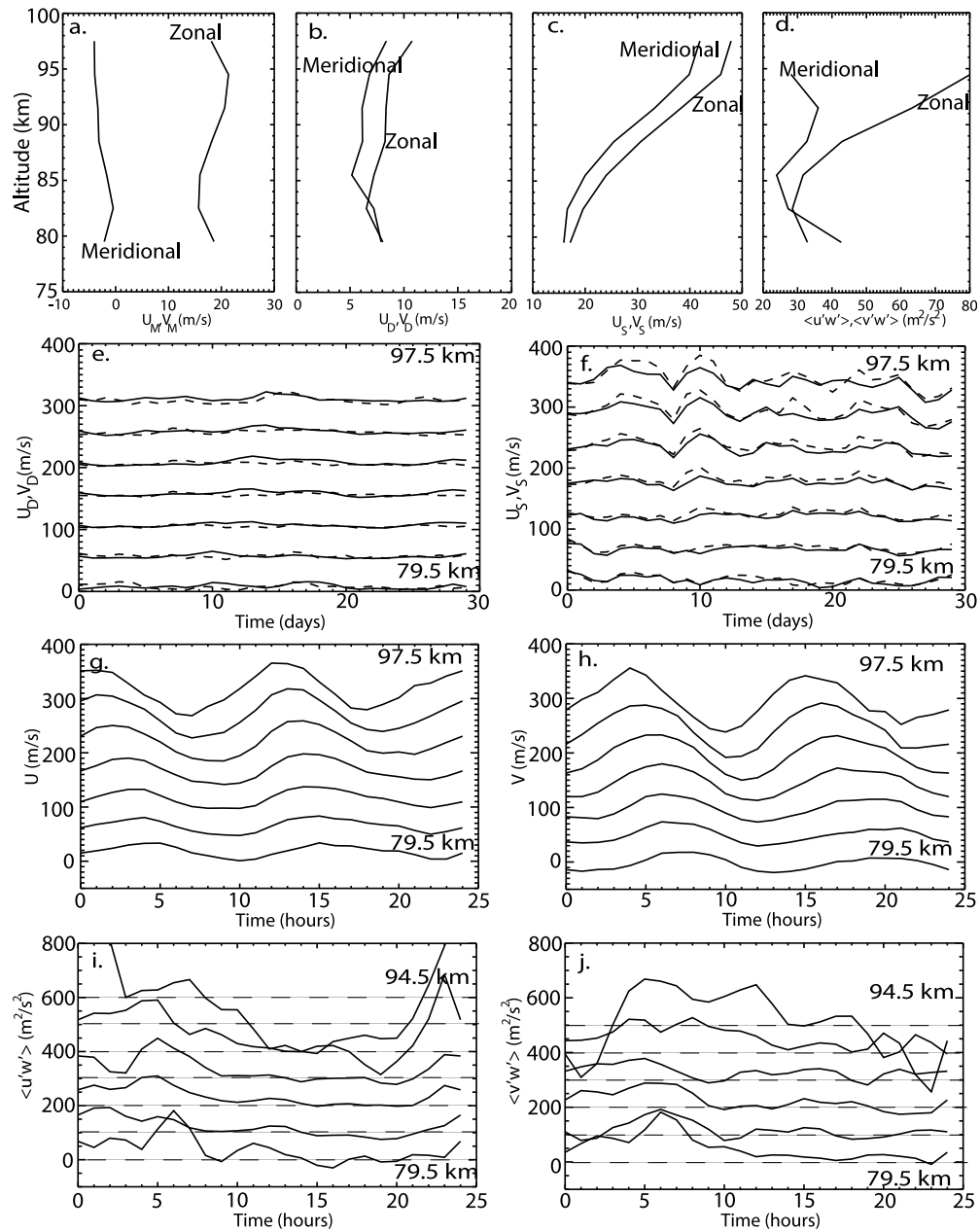


**Figure 15.** As in Figure 10, but for June 2009.

these times. Because of the weaker tidal motions than seen in June and September 2008, and perhaps also the lack of strong local GW sources at lower altitudes, we also see smaller and less systematic hourly variations in the momentum fluxes at intermediate altitudes (82.5–91.5 km) sampled throughout the composite day for March 2009.

### 3.5. June 2009 Data

[48] SAAMER measurements during two winter seasons allow us to also examine interannual variations in the motion fields. The June 2009 fields are displayed in Figure 15 and reveal strong overall similarities to those discussed above for June 2008. Mean zonal and meridional winds (top left frame of Figure 15) are again entirely eastward and southward during 2009, with the zonal winds  $\sim 10 \text{ m s}^{-1}$  weaker than

during June 2008 below  $\sim 80 \text{ km}$  and  $5\text{--}10 \text{ m s}^{-1}$  stronger at  $\sim 90 \text{ km}$  and above (see Figure 10). Mean meridional winds during June 2009 are  $\sim 5 \text{ m s}^{-1}$  weaker below  $\sim 85 \text{ km}$  and somewhat stronger above. These differences are well within the significant variations imposed by PW motions during winter discussed above and by F10. Tidal amplitudes, phases, and the magnitudes and periods of daily variations are nearly identical between June 2008 and 2009 as well. The most significant difference is an increase of only the zonal semi-diurnal amplitude by  $\sim 10 \text{ m s}^{-1}$  at the highest altitudes from 2008 to 2009.

[49] Turning now to the GW momentum flux estimates, we see that zonal and meridional mean values for June 2009 at 79.5 and 82.5 km ( $\sim 40$  and  $30 \text{ m}^2 \text{ s}^{-2}$ , respectively, with the smaller values at 82.5 km having greater confidence) are

very similar to those measured during June 2008. Both 2008 and 2009 zonal and meridional momentum flux profiles also exhibit minima of  $\sim 20\text{--}30\text{ m}^2\text{ s}^{-2}$  at  $\sim 82\text{--}85\text{ km}$  and then increase again to  $\sim 90\text{ km}$  or above. As seen above, we tend to distrust the momentum flux estimates at  $94.5\text{ km}$  in the presence of very large semidiurnal tidal motions, as the June 2009 amplitudes both exceed  $40\text{ m s}^{-1}$  at this altitude and above and are the largest mean tidal amplitudes reported here. The general agreement of the momentum flux profiles obtained during June 2008 and 2009 at intermediate altitudes nevertheless reinforces the arguments made above about the likely strong GW sources over the Drake Passage during austral winter and suggest their potential to influence MLT dynamics and variability in ways that remain to be studied in detail.

#### 4. Discussion

[50] SAAMER measurements of monthly mean winds and momentum fluxes discussed above reveal similarities to, but also some significant differences from, similar MLT measurements at other sites. Previous long-term measurements enabling correlations of mean winds and momentum fluxes in the MLT have been reported using three midlatitude and high-latitude radars: the MF radar at Adelaide, Australia [Vincent and Reid, 1983; Reid and Vincent, 1987; Fritts and Vincent, 1987; Murphy and Vincent, 1993], the former VHF radar at Poker Flat, Alaska [Fritts and Yuan, 1989; Wang and Fritts, 1990, 1991], and the MU VHF radar at Shigaraki, Japan [Tsuda et al., 1990; Nakamura et al., 1993]. Summer and winter measurements at these sites yielded zonal momentum fluxes consistently opposed (having the opposite sign) to the mean zonal wind. These momentum fluxes typically had magnitudes from a few to  $10$  or  $20\text{ m}^2\text{ s}^{-2}$ , with the higher values most often occurring for stronger mesospheric zonal winds and at the higher altitudes sampled. Notably, however, none of these sites coincides with the various “hot spots” of stratospheric GW variances observed in satellite measurements during different seasons.

[51] SAAMER measurements during November 2008 and March 2009, which are the only measurements discussed here that do not occur during the observed “hot spot” of stratospheric activity centered over the Drake Passage, follow the trends seen at other sites, with mean zonal winds largely anticorrelated with zonal momentum fluxes. The westward zonal jet having a maximum of  $\sim 43\text{ m s}^{-1}$  at  $\sim 80\text{ km}$  in November (Figure 13) is strongly anticorrelated with the zonal momentum flux having a magnitude of  $\sim 20\text{ m}^2\text{ s}^{-2}$  from  $\sim 80$  to  $85\text{ km}$  and a smaller magnitude above. The developing eastward jet in March 2009 at  $\sim 85\text{ km}$  and below is likewise largely opposed by the westward momentum flux of  $\sim -5\text{ m}^2\text{ s}^{-2}$  at  $82.5\text{ km}$ , which becomes positive above  $\sim 89\text{ km}$ . These observations appear largely consistent with measurements elsewhere. What are not consistent with measurements at other sites are the relatively large meridional momentum fluxes measured by SAAMER (negative, or southward, in November and positive, or northward, in March) in the presence of quite weak mean meridional winds. As noted above, these relatively large momentum fluxes, up to  $\sim -10$  to  $-40$  and  $\sim 20$  to  $30\text{ m}^2\text{ s}^{-2}$  during November 2008 and March 2009, suggest significant GW sources to the north and south of SAAMER during these times.

[52] SAAMER winter measurements during June 2008 and 2009 and September 2008, in contrast to those at Poker Flat ( $65^\circ\text{N}$ ), Adelaide ( $35^\circ\text{S}$ ), and SAAMER measurements during November 2008 and March 2009, exhibit correlated, rather than anticorrelated, zonal winds and momentum fluxes at altitudes from  $\sim 79.5$  to  $91.5\text{ km}$ . Indeed, the associated momentum flux divergences suggest a local acceleration of the mean zonal wind and a force balance that may be expressed as

$$dU/dt - fV \sim -(1/\rho)d(\rho\langle u'w' \rangle)/dz, \quad (5)$$

where  $U$  and  $V$  are the local mean zonal and meridional motions,  $f$  is the Coriolis parameter,  $\rho$  is density, and angle brackets denote a local spatial or temporal average. Thus the positive and decreasing zonal momentum fluxes in June 2008 and 2009 imply an acceleration, rather than a deceleration, of the mean zonal flow at these altitudes, at least locally, even if this is not the case averaged zonally. This implied acceleration is typically opposed by the Coriolis torque acting on the mean meridional wind ( $fV$ ) for quasi-steady mean motions with  $dU/dt \sim 0$  (see below).

[53] Two other, arguably robust, observations by SAAMER also suggest that these correlated mean winds and momentum fluxes may be reasonable, despite their lack of agreement with measurements elsewhere. First, the mean zonal winds observed by SAAMER during June 2008 and 2009 and September 2008 (and throughout each winter) extend to much higher altitudes with larger positive amplitudes than seen at the conjugate site of Juliusruh, Germany (D. C. Fritts, H. Iimura, D. Janches, and W. Singer, A conjugate study of mean winds, tides, and planetary waves employing enhanced meteor radars at Rio Grande, Argentina ( $52.8^\circ\text{S}$ ) and Juliusruh, Germany ( $54.6^\circ\text{N}$ ), submitted to *J. Geophys. Res.*, 2010, hereafter F11), suggesting a weaker and/or higher deceleration of the winter jet over SAAMER that may not be representative of a zonal average. Second, large mean meridional winds required to balance the momentum flux divergence term in equation (5) for steady mean motions [Holton, 1982; Garcia and Solomon, 1985; McIntyre, 1989] are seen to occur at significantly higher altitudes over SAAMER than over Juliusruh (F11) and are likely also not representative of a zonal average. Together, these observations suggest that there are systematic differences between SAAMER winter measurements and those at other sites, and that we should perhaps expect departures from the wind and momentum flux correlations seen elsewhere under very different GW forcing conditions in the lower atmosphere.

[54] Finally, we note that large local GW momentum flux estimates, either accompanying tidal modulation [Fritts and Vincent, 1987; Wang and Fritts, 1991; Espy et al., 2004], arising from specific sources [Espy et al., 2006; Smith et al., 2009], or having no identified cause [Fritts et al., 2002] often occur in the MLT. These estimates can significantly exceed the mean values reported at various sites, occasionally by one or two decades. Thus, it is not surprising that large monthly mean values can also occur in regions of demonstrated strong local GW sources, as appears to be the case over SAAMER, both during austral winter and in other seasons where other strong sources may also occur. Nevertheless, our initial SAAMER MLT momentum flux measurements require further verification and investigation of the GW sources and

propagation conditions contributing to their seasonal variations and implied MLT influences. We anticipate both a more complete assessment of seasonal and inter-annual momentum flux variations employing our first 2 years of observations and specific case studies when correlative instrumentation enables a more complete definition of the GW and large-scale motions in this region.

## 5. Summary and Conclusions

[55] We have presented an initial analysis of GW momentum fluxes in the MLT employing the Southern Argentina Agile Meteor Radar (SAAMER) that was installed at Rio Grande on Tierra del Fuego (53.8°S, 67.8°W) in May 2008. SAAMER was specifically designed with the hope that it would offer a new generation GW momentum flux measurement capability. This paper provides a series of tests of this capability with specified wind fields and observed SAAMER meteor distributions to confirm its ability to retrieve these specified wind fields and GW momentum fluxes. We then employ the same analysis methods to perform real SAAMER mean and tidal wind and GW momentum flux measurements for representative solstice and equinox periods throughout the first 17 months of observations.

[56] Specified test fields included seven cases having various combinations of the following:

[57] 1. zonal and meridional mean winds;

[58] 2. diurnal and semidiurnal tides assumed to rotate counterclockwise with time, with a diurnal tide that is constant in altitude and time and a semidiurnal tide that is either constant or varies with altitude and time;

[59] 3. traveling GWs having zonal, meridional, and/or oblique propagation, spatial and temporal variability, correlated horizontal and vertical motions, and constant and variable momentum fluxes; and/or

[60] 4. stationary GWs having zonal and meridional propagation, only spatial variability, correlated horizontal and vertical motions, and constant momentum fluxes.

[61] The retrieved fields indicate a SAAMER ability to define monthly mean and tidal wind fields very well at all altitudes for which meteor detection rates are sufficiently high, typically from 79.5 to 97.5 km (Cases 1 and 4–7). Monthly GW momentum fluxes for constant stationary or propagating GW fields were also retrieved with high accuracy (errors of a few percent) from 79.5 to 94.5 km with and without mean and tidal fields having large amplitudes (with the largest errors at 79.5 or 94.5 km in each case). In the presence of a semidiurnal tide that grew strongly in altitude and was strongly modulated at a 10 day period, GW momentum flux estimates exhibited larger errors over these altitudes, depending on the averaging period employed. Errors became smaller as the averaging interval increased from 1 to 3 to 10 days and were still within a few percent and a few  $\text{m}^2 \text{s}^{-2}$  for the larger mean zonal momentum flux of  $100 \text{ m}^2 \text{s}^{-2}$ , with comparable errors of a few  $\text{m}^2 \text{s}^{-2}$  in the meridional estimate.

[62] The greatest challenge for the SAAMER momentum flux measurement strategy proved to be transient GW packets having durations from 1 to 4 h, short periods of 15–30 min, random distributions throughout the diurnal cycle, and opposing contributions to the net GW momentum flux in some direction. These capabilities were assessed in Cases 6 and 7,

where mean momentum fluxes tended to be underestimated by ~5%–10%, with variability around these means from ~10% to 20% underestimates to ~10% overestimates, with the larger variability and uncertainties occurring when GWs make both positive and negative contributions to the mean momentum flux (as in the meridional component in Case 7). The larger uncertainties accompanying transient GW packets are nevertheless judged to be sufficiently small to allow useful SAAMER measurements where momentum flux magnitudes are large.

[63] Applications of the same analysis method to SAAMER measurements during June, September, and November 2008 and March and June 2009 were then examined in detail. These revealed mean winds that were preferentially eastward, except for a short interval of westward mean flow at lower altitudes (consistent with those reported by F10, with stronger eastward winds extending to higher altitudes than observed in conjugate winter measurements at Juliusruh, Germany (F11). Mean meridional winds were  $\sim 5 \text{ m s}^{-1}$  or less, except for estimates of  $\sim -10 \text{ m s}^{-1}$  below 80 km during June 2008 and above 90 km during September 2008. Estimates of mean diurnal tidal amplitudes were typically between  $\sim 5$  and  $13 \text{ m s}^{-1}$  at all altitudes in each measurement interval. Greater variability was seen in the mean semidiurnal tidal winds, which were seen to increase from  $\sim 10$  to  $15 \text{ m s}^{-1}$  at 79.5 km to  $\sim 35$  to  $45 \text{ m s}^{-1}$  at 94.5 km during June and September 2008 and June 2009, with smaller amplitudes of  $\sim 20$  and  $25 \text{ m s}^{-1}$ , respectively, during November 2008 and March 2009. In all months examined, much greater daily variability was seen in the semidiurnal than in the diurnal tide.

[64] Monthly mean GW momentum fluxes estimated from SAAMER measurements were found to exhibit a range of variability and correlations with mean winds. During November 2008 and March 2009, when the “hot spot” of stratospheric variance centered over the Drake Passage was not present, estimated zonal momentum fluxes were smaller and largely anticorrelated with mean zonal winds, with momentum flux magnitudes generally consistent with previous radar measurements at other midlatitude and high-latitude sites (including Adelaide, Australia, Shigaraki, Japan, and Poker Flat, Alaska). Mean meridional momentum fluxes during these same times, however, were larger than measured at these other sites, suggesting persistent, but as yet unidentified, local GW sources during these times.

[65] Mean GW momentum fluxes estimated with SAAMER during June and September 2008 and June 2009 differ significantly from measurements with other radars, both in their magnitudes and in their apparent correlations, rather than anticorrelations, with the mean winds. However, these measurements accompanied the very large stratospheric GW variances observed by various satellite instruments that are typically centered over the Drake Passage (and/or the adjacent Andes and Antarctic Peninsula) during these times throughout the austral winter season. In these cases, mean zonal winds remained eastward to higher altitudes than seen elsewhere, while mean meridional winds were weak and negative. Zonal momentum fluxes were large and positive,  $\sim 30 \text{ m}^2 \text{s}^{-2}$  or larger, at lower altitudes, and decreased to small or negative values above  $\sim 90$  km in June and September 2008. In contrast, zonal momentum fluxes during June 2009 were comparable at lower altitudes but increased strongly

above. Meridional momentum fluxes were large and positive during these 3 months, having magnitudes of  $\sim 15\text{--}50\text{ m}^2\text{ s}^{-2}$ , with the larger estimates occurring at the lowest and highest altitudes at which meteor statistics imply greater uncertainty. In each of these cases, our assessment of SAAMER momentum flux measurement capabilities suggests that these profiles and variability should be accurate to  $\sim 10\text{--}20\%$ , at least for those estimates having larger magnitudes.

[66] We interpreted the large and positive GW momentum fluxes (in both the zonal and meridional components) during austral winter as responses to strong GW generation accounting for the stratospheric variance enhancement in the Drake Passage “hot spot,” with apparent GW propagation away from the Drake Passage toward the northeast over SAAMER, thus explaining the positive zonal and meridional GW momentum fluxes in each case. Additional evidence that these momentum flux measurements and their departures from correlations with mean winds noted elsewhere are likely real includes (1) the extension of SAAMER mean eastward winds to higher altitudes and with larger magnitudes than seen at the conjugate site of Juliusruh, Germany, in winter and (2) corresponding observations of a significantly higher (in altitude) mean poleward wind over SAAMER than seen over Juliusruh in winter (F11). The larger mean zonal motions indicate a likely much smaller (or reversed) zonal GW drag (applying a westward body force) throughout the altitudes measured. The higher mean poleward circulation also indicates a higher zonal GW body than has been observed elsewhere. Together, these various fields suggest that SAAMER GW momentum flux measurements are largely internally consistent with parallel measurements of mean motions and that the MLT over the austral winter Drake Passage “hot spot” is a site of unique and strong coupling among the various motions occurring there.

[67] Finally, we noted in our examination of momentum fluxes throughout composite days that these tended to be reasonably coherent at tidal periods (except during March 2009) and to exhibit diurnal, rather than semidiurnal, variations, despite larger semidiurnal amplitudes at the higher altitudes. These results differ from the anticorrelations of momentum fluxes with the dominant tidal structures seen at other sites and with the strong semidiurnal modulation of GW variances by the semidiurnal tide observed with the meteor radar at Rothera at  $67.6^\circ\text{S}$  (C. L. Beldon and N. J. Mitchell, Gravity waves in the mesopause region observed by a meteor radar at Rothera ( $67.6^\circ\text{S}$ ): Evidence of semidiurnal modulation of gravity waves, submitted to *J. Geophys. Res.*, 2010). They nevertheless appear consistent with a similar assessment of GW variance modulation employing SAAMER, which indicates a primarily diurnal modulation (N. Mitchell, private communication, 2010). Together, these studies suggest that either the diurnal tide induces a diurnal modulation of GWs that depends more on other factors (e.g., vertical wavelength or temperature variations) than tidal winds or that there is a tidal modulation of GW sources at lower altitudes.

[68] Future studies will be required to diagnose these motion fields in greater detail and provide a quantitative assessment of the coupling of GWs from their sources at lower altitudes and their interactions with the mean, tidal, and PW motions in the MLT. We also anticipate additional evaluations of the SAAMER momentum flux measurement

capabilities employing meteor distributions observed at other times and additional mean, tidal, and GW fields exhibiting additional variability where these are suggested by additional SAAMER or other correlative measurements.

[69] **Acknowledgments.** The research described here was performed under NSF grants ATM-0634650 and ATM-0824742. We thank our colleague Ken Iimura for the plots displayed in Figure 11 and our colleagues at Genesis Software and MARDOC for their continuing efforts to assist us in enhancing SAAMER performance.

## References

- Acott, P. (2009), Mesospheric momentum flux studies over Fort Collins, CO, Ph.D. dissertation, Colorado State University.
- Ern, M., P. Preusse, M. J. Alexander, and C. D. Warner (2004), Absolute values of gravity wave momentum flux derived from satellite data, *J. Geophys. Res.*, *109*, D20103, doi:10.1029/2004JD004752.
- Espy, P. J., G. O. L. Jones, G. R. Swenson, and M. J. Taylor (2004), Tidal modulation of the gravity-wave momentum flux in the Antarctic mesosphere, *Geophys. Res. Lett.*, *31*, L11111, doi:10.1029/2004GL019624.
- Espy, P. J., R. E. Hibbins, G. R. Swenson, J. Tang, M. J. Taylor, D. M. Riggan, and D. C. Fritts (2006), Regional variations of mesospheric gravity-wave momentum flux over Antarctica, *Ann. Geophys.*, *24*, 81–88.
- Fritts, D. C., and L. Yuan (1989), Measurement of momentum fluxes near the summer mesopause at Poker Flat, Alaska, *J. Atmos. Sci.*, *46*, 2569–2579.
- Fritts, D. C., and R. A. Vincent (1987), Mesospheric momentum flux studies at Adelaide, Australia: Observations and a gravity wave/tidal interaction model, *J. Atmos. Sci.*, *44*, 605–619.
- Fritts, D. C., T. Tsuda, T. E. VanZandt, S. A. Smith, T. Sato, S. Fukao, and S. Kato (1990), Studies of velocity fluctuations in the lower atmosphere using the MU radar: II. Momentum fluxes and energy densities, *J. Atmos. Sci.*, *47*, 51–66.
- Fritts, D. C., L. Yuan, M. H. Hitchman, L. Coy, E. Kudeki, and R. F. Woodman (1992), Dynamics of the equatorial mesosphere observed using the Jicamarca MST radar during June and August 1987, *J. Atmos. Sci.*, *49*, 2353–2371.
- Fritts, D. C., S. A. Vadas, and Y. Yamada (2002), An estimate of strong local gravity wave body forcing based on OH airglow and meteor radar observations, *Geophys. Res. Lett.*, *29*(10), 1429, doi:10.1029/2001GL013753.
- Fritts, D. C., D. Janches, H. Iimura, W. K. Hocking, N. J. Mitchell, B. Fuller, B. Vandepuer, J. Hormaechea, C. Brunini, and H. Levato (2010), Southern Argentina Agile Meteor Radar (SAAMER): System design and initial measurements of large-scale winds and tides, *J. Geophys. Res.*, doi:10.1029/2010JD013850, in press.
- Fukao, S., T. Sato, T. Tsuda, and S. Kato (1988), VHF Doppler radar determination of the momentum flux in the upper troposphere and lower stratosphere: Comparison between the three- and four-beam methods, *J. Atmos. Ocean. Tech.*, *5*, 57–69.
- Garcia, R. R., and S. Solomon (1985), The effect of breaking gravity waves on the dynamics and chemical composition of the mesosphere and lower thermosphere, *J. Geophys. Res.*, *90*(D2), 3850–3868, doi:10.1029/JD090iD02p03850.
- Hitchman, M. H., K. W. Bywaters, D. C. Fritts, L. Coy, and E. Kudeki (1992), Mean winds and momentum fluxes over Jicamarca, Peru during June and August 1987, *J. Atmos. Sci.*, *49*, 2372–2383.
- Hocking, W. K. (2005), A new approach to momentum flux determinations using SKiYMET meteor radars, *Ann. Geophys.*, *23*, 1–7.
- Holton, J. R. (1982), The role of gravity wave induced drag and diffusion in the momentum budget of the mesosphere, *J. Atmos. Sci.*, *39*, 791–799.
- Jacobi, Ch., K. Fröhlich, Y. Portnyagin, E. Merzlyakov, T. Solovjova, N. Makarov, D. Rees, A. Fahrudinova, V. Guryanov, D. Fedorov, D. Korotyshekin, J. Forbes, A. Pogoreltsev, and D. Kürschner (2009), Semi-empirical model of middle atmosphere wind from the ground to the lower thermosphere, *Adv. Space Res.*, *43*, 239–246.
- Janches, D., S. Palo, E. M. Lau, S. K. Avery, J. P. Avery, S. de la Peña, and N. A. Makarov (2004), Diurnal and seasonal variability of the meteor flux at the South Pole measured with radars, *Geophys. Res. Lett.*, *31*, L20807, doi:10.1029/2004GL021104.
- Janches, D., C. J. Heinselman, J. L. Chau, A. Chandran, and R. Woodman (2006), Modeling the global micrometeor input function in the upper atmosphere observed by high power and large aperture radars, *J. Geophys. Res.*, *111*, A07317, doi:10.1029/2006JA011628.
- Jiang, J. H., D. L. Wu, and S. D. Eckermann (2002), Upper Atmosphere Research Satellite (UARS) MLS observation of mountain waves

- over the Andes, *J. Geophys. Res.*, 107(D20), 8273, doi:10.1029/2002JD002091.
- Jiang, J. H., S. D. Eckermann, D. L. Wu, and D. Y. Wang (2006), Interannual variation of gravity waves in the Arctic and Antarctic winter middle atmosphere, *Adv. Space Res.*, 37, 2418–2423.
- McIntyre, M. E. (1989), On dynamics and transport near the polar mesopause in summer, *J. Geophys. Res.*, 94(D12), 14,617–14,628, doi:10.1029/JD094iD12p14617.
- McLamb, C., M. J. Alexander, and D. L. Wu (2000), Microwave Limb Sounder observations of gravity waves in the stratosphere: A climatology and interpretation, *J. Geophys. Res.*, 105(D9), 11,947–11,967, doi:10.1029/2000JD900097.
- Murayama, Y., T. Tsuda, and S. Fukao (1994), Seasonal variation of gravity wave activity in the lower atmosphere observed with the MU radar, *J. Geophys. Res.*, 99(D11), 23,057–23,069, doi:10.1029/94JD01717.
- Murphy, D. J., and R. A. Vincent (1993), Estimates of momentum flux in the mesosphere and lower thermosphere over Adelaide, Australia, from March 1985 to February 1986, *J. Geophys. Res.*, 98(D10), 18,617–18,638, doi:10.1029/93JD01861.
- Murphy, D. J., and R. A. Vincent (1998), Mesospheric momentum fluxes over Adelaide during the 2-day wave: Results and interpretation, *J. Geophys. Res.*, 103, 28,627–28,636.
- Nakamura, T., T. Tsuda, M. Yamamoto, S. Fukao, and S. Kato (1993), Characteristics of gravity waves in the mesosphere observed with the middle and upper atmosphere radar: 1. Momentum flux, *J. Geophys. Res.*, 98(D5), 8899–8910, doi:10.1029/92JD02978.
- Portnyagin, Yu., et al. (2004), Mesosphere/lower thermosphere prevailing wind model, *Adv. Space Res.*, 34(8), 1755–1762.
- Reid, I. M., and R. A. Vincent (1987), Measurements of mesospheric gravity wave momentum fluxes and mean flow accelerations at Adelaide, Australia, *J. Atmos. Terres. Phys.*, 49, 443–460.
- Reid, I. M., R. Rüster, P. Czechowsky, and G. Schmidt (1988), VHF radar measurements of momentum flux in the summer polar mesosphere over Andenes (69°N, 16°E), Norway, *Geophys. Res. Lett.*, 15(11), 1263–1266, doi:10.1029/GL015i011p01263.
- Sato, K. (1990), Vertical wind disturbances in the troposphere and lower stratosphere observed by the MU radar, *J. Atmos. Sci.*, 47, 2803–2817.
- Sato, K. (1993), Small-scale wind disturbances observed by the MU radar during the passage of Typhoon Kelly, *J. Atmos. Sci.*, 50, 518–537.
- Sato, K. (1994), A statistical study of the structure, saturation and sources of inertia-gravity waves in the lower stratosphere observed with the MU radar, *J. Atmos. Terres. Phys.*, 56, 755–774.
- Smith, S., J. Baumgardner, and M. Mendillo (2009), Evidence of mesospheric gravity-waves generated by orographic forcing in the troposphere, *Geophys. Res. Lett.*, 36, L08807, doi:10.1029/2008GL036936.
- Stockwell, R. G., L. Mansinha, and R. Lowe (1996), Localization of the complex spectrum: The S transform, *IEEE Trans. Signal Process.*, 44, 998–1001.
- Tsuda, T., Y. Murayama, M. Yamamoto, S. Kato, and S. Fukao (1990), Seasonal variation of momentum flux in the mesosphere observed with the MU radar, *Geophys. Res. Lett.*, 17(6), 725–728, doi:10.1029/GL017i006p00725.
- Vadas, S. L., and D. C. Fritts (2004), Thermospheric responses to gravity waves arising from mesoscale convective complexes, *J. Atmos. Solar Terres. Phys.*, 66, 781–804.
- Vadas, S. L., and D. C. Fritts (2009), Reconstruction of the gravity wavefield from convective plumes via ray tracing, *Ann. Geophys.*, 27, 147–177.
- VanZandt, T. E., S. A. Smith, T. Tsuda, D. C. Fritts, T. Sato, S. Fukao, and S. Kato (1990), Studies of velocity fluctuations in the lower atmosphere using the MU radar: Part I. Azimuthal anisotropy, *J. Atmos. Sci.*, 47, 39–50.
- Vincent, R. A., and I. M. Reid (1983), HF Doppler measurements of mesospheric momentum fluxes, *J. Atmos. Sci.*, 40, 1321–1333.
- Wang, D.-Y., and D. C. Fritts (1990), Mesospheric momentum fluxes observed by the MST radar at Poker Flat, Alaska, *J. Atmos. Sci.*, 47, 1511–1521.
- Wang, D.-Y., and D. C. Fritts (1991), Evidence of gravity wave-tidal interaction observed near the summer mesopause at Poker Flat, Alaska, *J. Atmos. Sci.*, 48, 572–583.
- Wu, D. L. (2004), Mesoscale gravity wave variances from AMSU-A radiances, *Geophys. Res. Lett.*, 31, L12114, doi:10.1029/2004GL019562.
- Wu, D. L., and J. H. Jiang (2002), MLS observations of atmospheric gravity waves over Antarctica, *J. Geophys. Res.*, 107(D24), 4773, doi:10.1029/2002JD002390.

D. C. Fritts and D. Janches, NorthWest Research Associates, Colorado Research Associates Division, Boulder, CO, 80301, USA. (dave@cora.nwra.com)

W. K. Hocking, Department of Physics, University of Western Ontario, London, ON N6A 3K7, Canada.